

Controlled disagreement improves generalization in decentralized training

Zesen Wang¹ Mikael Johansson¹

Abstract

Decentralized training is often regarded as inferior to centralized training because the consensus errors between workers are thought to undermine convergence and generalization, even with homogeneous data distributions. This work challenges this view by introducing decentralized SGD with Adaptive Consensus (DSGD-AC), which intentionally preserves non-vanishing consensus errors through a time-dependent scaling mechanism. We prove that these errors are not random noise but systematically align with the dominant Hessian subspace, acting as structured perturbations that guide optimization toward flatter minima. Across image classification and machine translation benchmarks, DSGD-AC consistently surpasses both standard DSGD and centralized SGD in test accuracy and solution flatness. Together, these results establish consensus errors as a useful implicit regularizer and open a new perspective on the design of decentralized learning algorithms.

1. Introduction

In large-scale deep learning, decentralized optimization, where workers exchange model parameters only with neighbors, reduces the overhead of global synchronization and avoids costly global all-reduce communication (Abadi et al., 2016; Li et al., 2020). This neighbor-only exchange can substantially reduce communication overhead, latency, and single points of failure, making decentralized approaches attractive for geographically distributed systems (Dhasade et al., 2023; Gholami & Seferoglu, 2024) and even GPU clusters (Lian et al., 2017; Assran et al., 2019; Wang et al., 2025).

Despite its practical appeal in runtime efficiency, decentralized training methods such as Decentralized Stochastic Gradient Descent (DSGD) are conventionally viewed as suboptimal compared to centralized/synchronous SGD in

terms of convergence and, importantly, generalization performance even with i.i.d. data distributions among workers. This gap is largely attributed to consensus errors — persistent discrepancies in the model parameters maintained by different workers (Alghunaim & Yuan, 2022; Zhu et al., 2022). Prior work has focused heavily on minimizing these consensus errors to close the gap. Massive efforts have been made to reduce consensus errors, which involve communication topologies (Ying et al., 2021; Takezawa et al., 2023) and algorithm designs (Pu & Nedić, 2021; Wang et al., 2019; Lin et al., 2021) to ensure decentralized training closely approximates centralized training.

However, the conventional perspective neglects the potential constructive role of consensus errors. Rather than detrimental noise, these discrepancies may serve as structured perturbations that facilitate exploration of flatter minima in the loss landscape — solutions known to correlate with superior generalization (Jiang et al., 2019). This insight draws inspiration from sharpness-aware minimization strategies (Foret et al., 2020; Bisla et al., 2022; Li et al., 2024b), which explicitly introduce curvature-aware perturbations to enhance model robustness and performance.

In this study, we challenge the conventional view by introducing Decentralized SGD with Adaptive Consensus (DSGD-AC), an algorithm that strategically preserves non-vanishing consensus errors through an adaptive, time-dependent scaling mechanism. We provide a theoretical analysis demonstrating that consensus errors align with the dominant subspace of the Hessian matrix, thereby inducing beneficial curvature-related perturbations from the global average. DSGD-AC incurs negligible additional computational overhead relative to standard SGD or DSGD, while retaining the communication efficiency and runtime advantages of decentralized training.

Comprehensive experiments reveal that DSGD-AC consistently surpasses both DSGD and centralized SGD in terms of test accuracy and the flatness of the attained minima. To the best of our knowledge, this is the first demonstration that a decentralized training method outperforms centralized SGD even when the latter is optimally tuned.

The main contributions of this work are: (1) the proposal of DSGD-AC, an adaptive consensus algorithm that maintains theoretically-justified non-vanishing consensus errors

¹Division of Decision and Control Systems, KTH Royal Institute of Technology, Sweden. Correspondence to: Zesen Wang <zesen@kth.se>.

at minimal computational expense, (2) a theoretical characterization of consensus error and its alignment with the dominant Hessian subspace, and (3) empirical validation of the superior generalization performance of DSGD-AC on typical deep learning tasks.

1.1. Related work

Canonical view about consensus errors The prevailing view in decentralized training is that models should approximate centralized training as closely as possible. To mitigate discrepancies among local models caused by weakly connected networks, prior work has focused on tracking global information (Wang et al., 2019; Pu & Nedić, 2021; Yuan et al., 2021; Takezawa et al., 2022), enhancing communication topologies to improve convergence rates (Ying et al., 2021; Zhu et al., 2022; Takezawa et al., 2023), and more. In addition, several theoretical studies (Zhu et al., 2022; Alghunaim & Yuan, 2022) establish a theoretical connection between the connectivity of decentralized communication topologies and both convergence and generalization, demonstrating that weaker connectivity results in poorer outcomes on both fronts. In contrast, we demonstrate the potential advantages of the consensus error by identifying its correlation with the dominant Hessian subspace, and we propose DSGD-AC in which consensus errors can, in practice, outperform SGD in deep learning tasks.

Explorations beyond the canonical view While the canonical perspective dominates, research into the potential benefits of consensus errors remains sparse. (Kong et al., 2021) empirically identified error thresholds and noted advantages in specific training phases; however, they did not explore regimes where errors exceed those of ring-topology DSGD, and their control scheme showed limited gains. (Zhu et al., 2023) offers a novel interpretation, framing consensus errors in DSGD as random perturbations around the global average, which are asymptotically equivalent to average-direction SAM (Bisla et al., 2022). Our work further identifies the intrinsic curvature-related property of the consensus errors, and, by proposing DSGD-AC, empirically demonstrates the superior potential of decentralized training over centralized training without being limited to the large-batch setting.

Explicit curvature-related perturbations improve generalization but are costly With the idea of taking the global average as the deployed model (Zhu et al., 2023), decentralized learning can be interpreted as the learning on the (virtual) global average with the workers as the perturbed global average. Sharpness-aware minimization (SAM) was first proposed by (Foret et al., 2020) to improve the generalization of deep neural networks, and many variants (Kwon et al., 2021; Bisla et al., 2022; Liu et al., 2022; Li et al.,

2024a; Luo et al., 2024) were developed to further improve SAM. However, to achieve the best performance, the algorithms typically require one or more additional rounds of gradient evaluations, which significantly increase the computational costs. Our work utilizes the potential of the consensus errors as free perturbations to enhance the generalization without introducing extra computation.

2. Problem setting and notation

We consider decentralized training in GPU clusters where the full dataset is accessible to all workers within a single data-center infrastructure. Training uses a standard distributed data sampler: at the beginning of each epoch, the dataset is reshuffled and evenly partitioned across workers, yielding i.i.d. data distributions in expectation. This setting corresponds to the standard decentralized optimization regime studied in (Assran et al., 2019; Ying et al., 2021; Kong et al., 2021; Zhu et al., 2023; Wang et al., 2025).

Decentralized optimization. We consider a standard decentralized optimization setup where n workers collaborate to train a d -dimensional model. Let $[n]$ denote the set of integers $\{1, 2, \dots, n\}$. Each worker $i \in [n]$ holds a local objective determined by its local dataset \mathcal{D}_i :

$$f_i(x) = \mathbb{E}_{s \sim \mathcal{D}_i}[f_i(x; s)]. \quad (1)$$

The global optimization problem can be written as

$$\begin{aligned} \underset{\{x_1, x_2, \dots, x_n\}}{\text{minimize}} \quad & F(x_1, \dots, x_n) = \frac{1}{n} \sum_{i=1}^n f_i(x_i), \\ \text{subject to} \quad & x_i = x_j, \forall i, j \in [n], \end{aligned} \quad (2)$$

which enforces a hard consensus constraint across workers. In the i.i.d. data distribution setting considered in this work, all workers share the same underlying objective function, i.e., $f_i = f_j = F$ for all $i, j \in [n]$, while still operating on different data samples through independent minibatches drawn from the common dataset.

Decentralized SGD (DSGD) The update of DSGD (Lian et al., 2017) on worker i is:

$$\begin{aligned} x_i^{(t)} = & x_i^{(t-1)} - \alpha^{(t)} \nabla f(x_i^{(t-1)}; s_i^{(t)}) \\ & + \sum_{j \in \mathcal{N}(i)} W_{ij} (x_j^{(t-1)} - x_i^{(t)}) \end{aligned} \quad (3)$$

where $\mathcal{N}(i)$ is the set of neighbors of worker i (including itself), W is a symmetric, non-negative, and doubly stochastic matrix defining the weights of the edges ($W_{ij} = 0$ if worker i is not a neighbor of worker j), and $s_i^{(t)}$ denotes the stochastic mini-batch sampled by worker i at iteration t .

Following the common notation in decentralized optimization, we denote the global average by

$\bar{x}^{(t)} := \sum_{i=1}^n x_i^{(t)}$, the consensus error of worker i by $e_i^{(t)} := x_i^{(t)} - \bar{x}^{(t)}$, the matrix form of all local models by $X^{(t)} := [x_1^{(t)}, \dots, x_n^{(t)}] \in \mathbb{R}^{d \times n}$, the matrix form of all local stochastic gradients by $G^{(t)} := [\nabla f_1(x_1^{(t-1)}; s_1^{(t)}), \dots, \nabla f_n(x_n^{(t-1)}; s_n^{(t)})]$, the matrix form of all consensus errors as $\Delta^{(t)} = [e_1^{(t)}, \dots, e_n^{(t)}]$, and the matrix \bar{X} by $\bar{X}^{(t)} = [\bar{x}^{(t)}, \dots, \bar{x}^{(t)}]$.

Note that there is another variant of DSGD that performs the local update before communication. We focus on the variant in Eq. (3) as it is shown to be more efficient (Lian et al., 2017; Wang et al., 2025), and two variants are proven to have the same generalization bound (Bellet et al., 2023).

3. DSGD-AC: DSGD with adaptive consensus

In this section, we use the experiment of training a wide ResNet (WRN28-10) (Zagoruyko & Komodakis, 2016) on CIFAR-10 (Krizhevsky et al., 2009) as a showcase to demonstrate the limitation of DSGD and the improvement brought by our proposed algorithm. In the experiment, we employ the standard cosine annealing learning rate schedule (Loshchilov & Hutter, 2016) with a linear warm-up during the first 10 epochs (Figure 1a). This learning rate schedule is commonly used in deep neural network training for better training stability and generalization (Gotmare et al., 2018; Kalra & Barkeshli, 2024). For decentralized training, we use 8 workers and the one-peer ring as the decentralized communication topology.

3.1. Finding: vanishing consensus error in DSGD

We start by empirically investigating the dynamics of consensus errors when trained with DSGD. We track the average norm of the consensus errors during the training. We observe that, for DSGD, the consensus errors gradually vanish as the learning rate decreases (Figure 1b).

From the theoretical perspective, by interpreting the mixing step as a gradient step on a quadratic consensus penalty, one obtains the per-step surrogate

$$\begin{aligned}
 J^{(t)}(x_1, \dots, x_n) &= \sum_{i=1}^n f_i(x_i^{(t)}) + \frac{1}{2\alpha^{(t)}} \sum_{i,j \in [n]} W_{ij} \|x_i^{(t)} - x_j^{(t)}\|^2 \\
 &= \underbrace{\sum_{i=1}^n f_i(\bar{x}^{(t)})}_{\text{objective on deployed model}} + \underbrace{\sum_{i=1}^n [f_i(x_i^{(t)}) - f_i(\bar{x}^{(t)})]}_{\text{sharpness}} \\
 &\quad + \underbrace{\frac{1}{2\alpha^{(t)}} \sum_{i,j \in [n]} W_{ij} \|x_i^{(t)} - x_j^{(t)}\|^2}_{\text{consensus regularizer}}
 \end{aligned} \tag{4}$$

With symmetric mixing weights and no momentum or adaptivity, each DSGD step is exactly a (stochastic) gradient on

J . Thus, when $\alpha^{(t)}$ goes to 0, the consensus regularizer dominates the objective function, which minimizes the consensus errors. If considering this surrogate function, the empirical observation is not surprising because it reflects the hard constraint in the optimization problem in Eq. (2). However, the vanishing consensus errors void the sharpness term in Eq. (4) because the sharpness term becomes $f_i(x_i^{(t)}) \approx f_i(\bar{x}^{(t)})$ as $x_i^{(t)} - \bar{x} \rightarrow 0$. The only term left that is relevant to the deployed model $\bar{x}^{(t)}$ is the first term, which is the same objective as in synchronous SGD. Therefore, to maintain the potential benefits of free sharpness-aware regularization (Zhu et al., 2023) by the consensus errors, we need to maintain a non-vanishing radius throughout the training.

3.2. Algorithm: DSGD with adaptive consensus

The proposed algorithm is shown in Algorithm 1. The difference from DSGD is highlighted, and, compared with DSGD, the proposed variant includes an adaptive factor to maintain non-diminishing consensus errors intentionally. At the end of training, the algorithm takes the global average of all local models as the deployed model.

Algorithm 1: Decentralized SGD with adaptive consensus (DSGD-AC) on worker i

Data: Dataset (D), the number of workers (N), the number of epoch (E), the number of batches per epoch (T), initialization ($x^{(0)}$), and a hyperparameter ($p \in \mathbb{R}^+$).

Result: Deployed model $\bar{x} = \frac{1}{n} \sum_{j=1}^n x_j^{(TE)}$

$$\begin{aligned}
 x_1^{(0)} &= x_2^{(0)} = \dots = x_n^{(0)} = x^{(0)} \\
 \text{for } t = 1 \text{ to } TE \text{ do} \\
 &\quad \left| \begin{aligned}
 g_i^{(t)} &= \nabla f(x_i^{(t-1)}; s_i^{(t)}) \\
 \gamma^{(t)} &= [\alpha^{(t)}/\alpha_{\max}]^p \\
 x_i^{(t)} &= x_i^{(t-1)} - \\
 &\quad \alpha^{(t)} g_i^{(t)} + \gamma^{(t)} \sum_{j \in \mathcal{N}(i)} W_{ij} (x_j^{(t-1)} - x_i^{(t-1)})
 \end{aligned} \right. \\
 \text{end}
 \end{aligned}$$

Note that $\alpha^{(t)}$ is determined by the learning rate scheduler like cosine annealing (Loshchilov & Hutter, 2016), and α_{\max} is the maximal learning rate throughout the training, which ensures $\gamma^{(t)}$ is in the range $[0, 1]$.

We evaluate the performance of DSGD-AC on classical deep learning tasks in Section 4. In the numerical experiments, the results demonstrate the superior generalization performance of DSGD-AC over DSGD and centralized SGD. We will analyze the reasons behind this by showing that DSGD-AC maintains non-diminishing and useful consensus errors in the following sections.

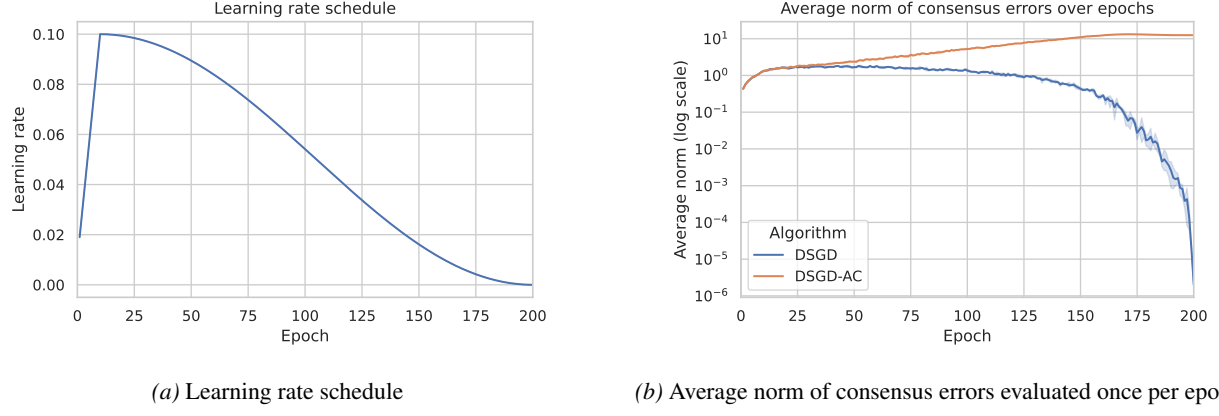


Figure 1. Decentralized training of WRN28-10 on CIFAR-10 with 8 workers and the one-peer ring topology. $p = 3$ for DSGD-AC.

3.3. Controlled consensus errors in DSGD-AC

The motivation of DSGD-AC is to maintain non-diminishing consensus errors. Therefore, we multiply the weight of the consensus regularizer in Eq. (4) by an adaptive γ , which directly leads to the DSGD-AC algorithm. The per-step surrogate function of DSGD-AC is mostly the same as that of DSGD. Only the weight of the consensus regularizer becomes $\gamma^{(t)}/(2N\alpha^{(t)})$.

In this section, we investigate the impact of p on the magnitude of consensus errors. First, we can rewrite the update of DSGD-AC in matrix form,

$$\begin{aligned} X^{(t)} &= X^{(t-1)} - \alpha^{(t)} G^{(t)} - \gamma^{(t)} X^{(t-1)}(I - W) \\ &= X^{(t-1)}(I - \gamma^{(t)} L) - \alpha^{(t)} G^{(t)} \end{aligned} \quad (5)$$

where we denote the Laplacian matrix L by $L = I - W$.

By subtracting $\bar{X}^{(t)}$ on both sides of Eq. (5) and using the fact that $\Delta^{(t)} = X^{(t)}(I - \frac{1}{n}\mathbf{1}\mathbf{1}^\top)$, the dynamics of consensus errors $\Delta^{(t)}$ can be derived as

$$\begin{aligned} \Delta^{(t)} &= X^{(t-1)}(I - \gamma^{(t)} L) - \alpha^{(t)} G^{(t)} - \bar{X}^{(t)} \\ &= X^{(t-1)}(I - \gamma^{(t)} L) - \alpha^{(t)} G^{(t)} - \bar{X}^{(t-1)} \\ &\quad + \alpha^{(t)} G^{(t)} \cdot \frac{1}{n} \mathbf{1}\mathbf{1}^\top \\ &= \Delta^{(t-1)}(I - \gamma^{(t)} L) - \alpha^{(t)} G^{(t)}(I - \frac{1}{n}\mathbf{1}\mathbf{1}^\top) \end{aligned} \quad (6)$$

Next, we denote $P = I - \frac{1}{n}\mathbf{1}\mathbf{1}^\top$, perform an eigen-decomposition of $L = U_L \Lambda_L U_L^\top$, and multiply Eq. (6) by U_L from the right to obtain

$$\begin{aligned} \Delta^{(t)} U_L &= \Delta^{(t-1)}(I - \gamma^{(t)} U_L \Lambda_L U_L^\top) U_L - \alpha^{(t)} G^{(t)} P_L U_L \\ &= \Delta^{(t-1)} U_L (I - \gamma^{(t)} \Lambda_L) - \alpha^{(t)} G^{(t)} P_L U_L \end{aligned} \quad (7)$$

By introducing $Z^{(t)} = \Delta^{(t)} U_L$ and $\tilde{G}^{(t)} = G^{(t)} P_L U_L$, we can re-write the update as

$$Z^{(t)} = Z^{(t-1)}(I - \gamma^{(t)} \Lambda_L) - \alpha^{(t)} \tilde{G}^{(t-1)} \quad (8)$$

Here, $Z^{(t)}$ collects the consensus error expressed in the eigenbasis of the Laplacian. The k -th row $Z_k^{(t)}$ contains the coefficients of $\Delta^{(t)}$ along the k -th Laplacian eigenvector, or network mode, and thus describes a characteristic pattern of disagreement across agents induced by the communication graph. We measure the overall amount of disagreement by the disagreement radius

$$r_t^2 := \mathbb{E} \left[\|\Delta^{(t)}\|_F^2 \right].$$

Since U_L is orthogonal, $\|\Delta^{(t)}\|_F = \|Z^{(t)}\|_F$, so the radius can be equivalently studied through the Laplacian-mode dynamics of $Z^{(t)}$ in (8). By analyzing these dynamics, we obtain the following proposition; the proof is deferred to Section A.1 in the appendix.

Proposition 3.1 (Disagreement radius and the role of γ). *In a quasi-stationary regime with mild bounded-moment and spectral assumptions (see Appendix A.1) the disagreement radius satisfies*

$$r_t^2 = \Theta \left(\frac{(\alpha^{(t)})^2}{\gamma^{(t)}} \right)$$

In particular, if $\alpha^{(t)} \rightarrow 0$ and $\gamma^{(t)}$ is bounded away from zero, then $r_t^2 \rightarrow 0$. Thus, no constant $\gamma^{(t)}$ can maintain a non-vanishing disagreement radius as the step size diminishes. However, if we choose $\gamma^{(t)} = g_0 (\alpha^{(t)})^p$ for some $g_0 > 0$ and $p > 0$, then as $\alpha^{(t)} \rightarrow 0$, $r_t^2 = \Theta(1)$ if $p = 2$, which means $p \geq 2$ is necessary to keep the consensus errors at a nontrivial scale.

The proposition establishes that DSGD-AC maintains a non-trivial level of consensus errors throughout iterations. In

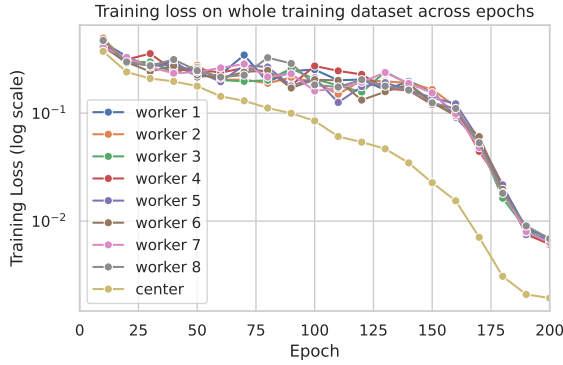


Figure 2. Losses on the whole training dataset at local workers and global average. The losses are evaluated every 10 epochs.

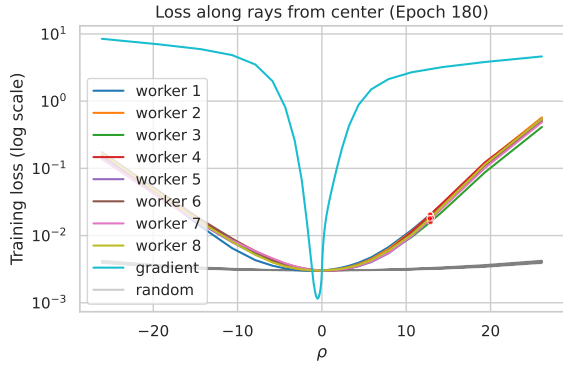


Figure 3. Training loss at epoch 180 along: (1) worker i : lines connecting global average and worker i , (2) gradient: the line that aligns with the full-batch gradient at the global average and crosses the global average, and (3) random: 500 lines that cross the global average and follow random directions generated as in (Bisla et al., 2022). The x -axis means the directional magnitude of the perturbation along these directions. The red dots represent the losses at the local models. The losses are computed on $\sim 1/4$ of the training dataset due to heavy computation complexity.

fact, the proof of the proposition shows that the effective disagreement radius $r_t^2 = \mathbb{E}[\|\Delta^{(t)}\|_F^2]$ is of order $(\alpha^{(t)})^2/\gamma^{(t)}$. Since it has been empirically observed (see, e.g., (Bisla et al., 2022; Li et al., 2024a)) that it is advantageous to increase the radius slightly towards the end of the training, we chose $\gamma^{(t)} = g_0(\alpha^{(t)})^p$ with $p = 3$. Under cosine learning rate schedules, this choice induces a mild uptick in the radius toward the final stages of training, as illustrated in Figure 1b. A detailed sensitivity analysis in Section 4.1 further supports the theory, demonstrating radius shrinkage for $p < 2$ and growth for $p > 2$ as $\alpha^{(t)} \rightarrow 0$ (see Figure 4).

3.4. Consensus errors align with dominant subspace of Hessian

Even though DSGD-AC maintains non-vanishing consensus errors, its role in leading to flatter minima and better generalization remains underexplored. In (Zhu et al., 2023, Theorem 1), consensus errors are interpreted as random perturbations within the subspace defined by the weight diversity matrix, and the resulting (asymptotically equivalent) average-direction SAM effect is shown to improve generalization. While this connection is insightful, the intrinsic structure of consensus errors (or the weight diversity matrix) has not been examined in detail.

To study this structure, we compare the training losses at local models with those at their global average. As shown in Figure 2, the global average consistently achieves lower training loss than any individual worker. To further distinguish consensus errors from random perturbations, we evaluate the training losses along the directions of consensus errors and compare them against losses along sufficiently many random directions. Figure 3 shows that the random directions are almost flat, which is expected given the large parameter space ($\sim 36M$ in WRN28-10) and the low-rank structure of the Hessian (Gur-Ari et al., 2018; Song et al., 2024). It is also consistent with empirical observations in (Keskar et al., 2016).

In contrast, directions induced by consensus errors yield significant increases in training loss, highlighting that these errors are not random but aligned with directions of higher curvature. This phenomenon suggests a correlation between consensus errors and the dominant subspace of the Hessian (or directions with larger curvature). Motivated by this observation, we formalize it in the following proposition, with the proof deferred to Appendix A.2.

Proposition 3.2 (Structure of consensus errors). *Let x^* be a locally strongly convex minimizer of F with Hessian $H = U_H \Lambda_H U_H^\top$ and eigenvalues $0 < \lambda_1(H) \leq \dots \leq \lambda_d(H)$. Assume i.i.d. local objectives $(f_i \equiv F)$, and let W be a symmetric, doubly stochastic communication matrix associated with a connected undirected graph. Let $\Delta^{(t)}$ denote the consensus error at time t . Consider the DSGD-AC recursion in a neighbourhood of x^* and approximate the local gradients by their first-order Taylor expansion, $\nabla f_i(x_i^{(t)}) \approx H(x_i^{(t)} - x^*)$. For non-increasing stepsizes $\alpha^{(t)} > 0$ and consensus factors $\gamma^{(t)} > 0$, the projection $\Delta_k^{(t)} := u_k^\top \Delta^{(t)}$ of the consensus error onto each Hessian eigenvector u_k then evolves as a scalar linear system whose stability requires*

$$\alpha^{(t)} < \frac{2 + (\lambda_{\min}(W) - 1) \gamma^{(t)}}{\lambda_k(H)}, \quad (9)$$

where $\lambda_{\min}(W)$ is the smallest eigenvalue of W . The right-hand side of (9) is decreasing in $\lambda_k(H)$, so with non-

increasing stepsizes $\alpha^{(t)}$ modes corresponding to smaller eigenvalues enter the stable regime earlier, while high-curvature modes remain closer to instability for longer and therefore retain higher variance under the same injected noise.

Remark 1 (Theoretical benefit of adaptive consensus)

A smaller consensus factor $\gamma^{(t)}$ relaxes the stability condition in (9). As $\gamma^{(t)}$ decreases during training, more low-curvature modes become stable, while the high-curvature modes remain closer to instability. As a result, the consensus errors gradually concentrate on a lower-dimensional subspace spanned by the dominant Hessian directions.

Remark 2 (Alignment is meaningful only with a controlled disagreement radius) The conclusion of Proposition 3.2 only holds when the disagreement radius stays in a reasonable range. Although one may relax the condition (9) by the selection of W and $\gamma^{(t)}$, taking $\gamma^{(t)}$ too small or using a graph with a very large $\lambda_{\min}(W)$ can cause the disagreement to grow quickly (Proposition 3.1). In that case, the iterates may move out of the region where the local Taylor approximation is accurate. On the other hand, if the radius becomes too small, the disagreement barely perturbs the model, and its directional structure becomes unimportant. Thus, the alignment effect is useful only when the disagreement radius is controlled.

To connect the result of Proposition 3.2 to the objective optimized by DSGD-AC, Appendix A.3 analyzes the deployed model $\bar{x}(t)$ and the disagreements $\delta_i^{(t)} = x_i^{(t)} - \bar{x}^{(t)}$. Using a second-order expansion of F around x^* , we show that

$$\frac{1}{N} \sum_{i=1}^N f_i(x_i^{(t)}) = F(\bar{x}(t)) + \frac{1}{2} \text{tr}(H\Sigma_t) + O((\text{tr} \Sigma_t)^{3/2}),$$

where Σ_t is the disagreement covariance. Thus, in this local regime, DSGD-AC can be interpreted as minimizing the central loss $F(\bar{x}(t))$ plus a Hessian-weighted disagreement penalty. A spectral decomposition of this penalty reveals that the mode weights are strictly increasing in the Hessian eigenvalues. Disagreement in sharper directions therefore incurs a larger penalty, resulting in a “curvature tilt” toward flatter minima; see Appendix A.3 for more details.

Given the alignment between the consensus errors and the dominant subspace, DSGD-AC can be interpreted as optimization over \bar{x} with curvature-correlated noises, which has been both empirically and theoretically studied by many works (Foret et al., 2020; Zhang et al., 2023; Luo et al., 2024; Benedetti & Ventura, 2024). By maintaining non-vanishing consensus errors along with its regularization effect on the curvature of the loss landscape, DSGD-AC is expected to achieve better generalization performance than DSGD and SGD.

While the alignment exists and can be shown theoretically,

the alignment is noisy and spans on less-sharp directions when compared with the gradient direction. As shown in Figure 3, the gradient computed on the corresponding dataset leads to a sharper increase than the consensus errors. An interesting direction for future work could be an improved algorithm based on DSGD-AC that can utilize the gradient information to promote the concentration of consensus errors on the dominant Hessian subspace with small computational overhead.

4. Numerical Experiments

In this section, we present extensive numerical experiments on image classification using Wide ResNets (Zagoruyko & Komodakis, 2016) trained on CIFAR-10 and CIFAR-100 (Krizhevsky et al., 2009) under a variety of distributed setups. We follow the hyperparameter settings from the original papers and reproduce comparable baseline performance to ensure fair comparisons. All models are trained for 200 epochs. The global batch size is set to 128 for 8 workers and is linearly scaled with the number of workers; mixed-precision training is enabled by default. Following Defazio et al. (2024)¹, we perform a calibration pass over the training set before evaluation to correct mismatches in batch normalization running statistics across workers, yielding more reliable test performance. Additional training and evaluation details are deferred to Appendix A.5.

Each experiment is repeated three times with fixed random seeds. We report mean \pm standard deviation, and shaded regions in plots indicate 95% confidence intervals.

Although not the primary focus of this work, Appendix A.4.1 reports additional experiments combining adaptive consensus with the Adam optimizer (Adam et al., 2014) for Transformer models (Vaswani et al., 2017) on WMT-14 (Bojar et al., 2014) to illustrate the potential of the proposed mechanism for improving adaptive optimization.

4.1. Ablation study and sensitivity analysis

Parameter p Table 2 presents the sensitivity analysis with respect to p . The results indicate that the best test accuracy and test loss are achieved for $p \in [2, 4]$. Since DSGD-AC reduces to DSGD when $p = 0$, these experiments also serve as an ablation study of the adaptive consensus mechanism. With $p \neq 0$, DSGD-AC always achieves better performance than DSGD. Figure 4 presents the average norm of the consensus errors with various p . Consistent with the analysis in Section 3.3, the consensus errors persist for $p \geq 2$.

Start epoch E_{start} We also tune the epoch (E_{start}) to activate the adaptive consensus mechanism. By default, we set

¹https://github.com/facebookresearch/schedule_free

Controlled disagreement improves generalization in decentralized training

Model	# W	Topo.	Algorithms (Test Accuracy (%) \uparrow / Test Loss \downarrow / Top-1 Eigenvalue \downarrow)		
			Synchronous SGD	Decentralized SGD	DSGD-AC (ours)
WRN28-10	8	ring		79.93 ± 0.23 / 1.108 ± 0.017 / 1.137 ± 0.761	81.98 ± 0.19 / 0.915 ± 0.011 / 0.426 ± 0.035
		exp	80.15 ± 0.29 / 1.100 ± 0.005 / 0.584 ± 0.114	79.57 ± 0.32 / 1.092 ± 0.016 / 1.143 ± 0.172	81.75 ± 0.13 / 0.916 ± 0.003 / 0.303 ± 0.020
		complete		79.69 ± 0.12 / 1.125 ± 0.011 / 1.089 ± 0.336	81.52 ± 0.19 / 0.956 ± 0.010 / 0.186 ± 0.064
	16	ring		80.34 ± 0.09 / 1.036 ± 0.003 / 0.789 ± 0.238	82.07 ± 0.28 / 0.840 ± 0.010 / 0.399 ± 0.017
		exp	79.76 ± 0.16 / 1.102 ± 0.009 / 0.953 ± 0.620	80.19 ± 0.20 / 1.060 ± 0.017 / 0.799 ± 0.253	82.03 ± 0.17 / 0.879 ± 0.001 / 0.295 ± 0.012
		complete		80.01 ± 0.48 / 1.093 ± 0.029 / 1.109 ± 0.429	81.60 ± 0.17 / 0.932 ± 0.006 / 0.156 ± 0.007
	32	ring		80.73 ± 0.09 / 0.957 ± 0.004 / 1.182 ± 0.643	81.93 ± 0.19 / 0.834 ± 0.008 / 0.364 ± 0.001
		exp	80.02 ± 0.13 / 1.089 ± 0.009 / 0.640 ± 0.352	80.45 ± 0.11 / 1.010 ± 0.004 / 0.730 ± 0.040	81.82 ± 0.19 / 0.883 ± 0.003 / 0.212 ± 0.015
		complete		80.34 ± 0.12 / 1.047 ± 0.021 / 1.919 ± 1.202	81.35 ± 0.18 / 0.924 ± 0.015 / 0.192 ± 0.017
WRN16-8	8	ring		79.02 ± 0.12 / 1.002 ± 0.004 / 0.635 ± 0.121	80.25 ± 0.27 / 0.903 ± 0.014 / 0.535 ± 0.011
		exp	79.07 ± 0.13 / 0.997 ± 0.006 / 0.425 ± 0.118	78.86 ± 0.24 / 0.995 ± 0.002 / 0.683 ± 0.389	80.32 ± 0.32 / 0.906 ± 0.001 / 0.500 ± 0.012
		complete		79.00 ± 0.31 / 0.997 ± 0.017 / 0.380 ± 0.201	80.20 ± 0.20 / 0.926 ± 0.001 / 0.338 ± 0.028
	16	ring		79.05 ± 0.10 / 0.980 ± 0.008 / 0.899 ± 0.336	80.63 ± 0.10 / 0.859 ± 0.005 / 0.474 ± 0.016
		exp	78.71 ± 0.24 / 1.019 ± 0.007 / 0.738 ± 0.340	78.86 ± 0.23 / 0.997 ± 0.002 / 0.421 ± 0.063	80.43 ± 0.21 / 0.882 ± 0.012 / 0.446 ± 0.002
		complete		79.06 ± 0.39 / 1.003 ± 0.012 / 0.403 ± 0.139	80.19 ± 0.18 / 0.922 ± 0.006 / 0.333 ± 0.022
	32	ring		79.17 ± 0.15 / 0.977 ± 0.017 / 0.492 ± 0.048	80.38 ± 0.09 / 0.880 ± 0.005 / 0.500 ± 0.009
		exp	78.88 ± 0.06 / 1.012 ± 0.001 / 0.672 ± 0.412	79.04 ± 0.21 / 0.980 ± 0.004 / 0.558 ± 0.064	80.04 ± 0.06 / 0.923 ± 0.007 / 0.339 ± 0.021
		complete		78.99 ± 0.13 / 0.999 ± 0.011 / 0.411 ± 0.178	79.85 ± 0.13 / 0.942 ± 0.012 / 0.257 ± 0.014

Table 1. Performance comparison of synchronous SGD, decentralized SGD, and DSGD-AC. Dataset: CIFAR-100. Model: WRN28-10 and WRN16-8. Number of workers: 8, 16, 32. Topology: one-peer ring, one-peer exponential graph (Ying et al., 2021), and complete graph. $p = 3$ for all DSGD-AC experiments. E_{start} is set to 10, 100 and 150 for 8-worker, 16-worker and 32-worker setups, respectively. The best metric values for the experiment setups are in **bold**.

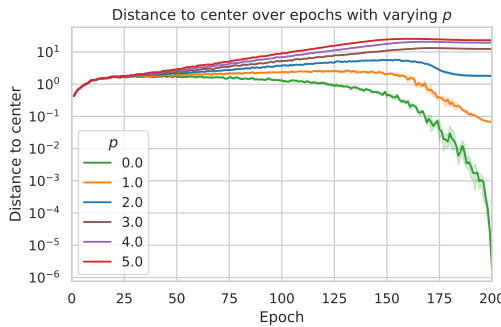


Figure 4. Average norm of consensus errors over epochs with varying p in the WRN28-10 on CIFAR-10 experiments with 8 workers and the one-peer ring topology.

$E_{\text{start}} = 10$, which is after the learning rate warm-up phase. In setups with more workers or weaker connectivity in the communication topology, decentralization itself already induces substantial consensus error in the early training phase. As shown in Table 3, tuning E_{start} enables a better trade-off between convergence and generalization. For the setup with 16 workers and the one-peer ring topology, $E_{\text{start}} = 100$ gives the best generalization performance for DSGD-AC.

Appendix A.4.4 and A.4.5 include more results on sensitivity analysis.

p	Test Accuracy (%) \uparrow	Train Loss \downarrow	Test Loss \downarrow
0	96.07 ± 0.13	0.002 ± 0.000	0.176 ± 0.005
1	96.26 ± 0.14	0.002 ± 0.000	0.159 ± 0.003
2	96.58 ± 0.18	0.003 ± 0.000	0.141 ± 0.006
3	96.77 ± 0.11	0.012 ± 0.000	0.128 ± 0.003
4	96.53 ± 0.13	0.024 ± 0.001	0.127 ± 0.004
5	96.37 ± 0.04	0.032 ± 0.001	0.130 ± 0.002

Table 2. Sensitivity analysis of parameter p in the WRN28-10 on CIFAR-10 experiments with 8 workers and one-peer ring topology.

4.2. Tuned results with various setups

In Table 1, we summarize the experiment results of DSGD-AC with tuned p and E_{start} , and the comparisons with SGD and DSGD in various setups. The algorithms are applied on training WRN28-10 and WRN16-8 on the CIFAR-100 dataset. The number of workers varies from 8 to 32, and the topologies are one-peer ring, one-peer exponential, and complete graph. According to the sensitivity analysis, we choose $p = 3$ for all DSGD-AC experiments, and $E_{\text{start}} = 10$, 100, and 150 for 8-worker, 16-worker, and 32-worker setups, respectively.

Since finding the best sharpness metric that always reflects the potential generalization is still an open question, we use the top-1 eigenvalue of the Hessian as a surrogate, which

E_{start}	Test Accuracy (%) \uparrow	Train Loss \downarrow	Test Loss \downarrow
10	96.16 ± 0.03	0.048 ± 0.001	0.122 ± 0.001
50	96.22 ± 0.04	0.039 ± 0.001	0.122 ± 0.003
75	96.37 ± 0.13	0.029 ± 0.001	0.123 ± 0.002
100	96.61 ± 0.07	0.017 ± 0.001	0.123 ± 0.001
150	96.39 ± 0.04	0.002 ± 0.000	0.153 ± 0.003
175	96.03 ± 0.17	0.001 ± 0.000	0.185 ± 0.007

Table 3. Sensitivity analysis of E_{start} in the WRN28-10 on CIFAR-10 experiments with 16 workers and one-peer ring topology.

# Nodes	SGD	DSGD	DSGD-AC
1	90.83 ± 0.22 ($\times 1.000$)	78.47 ± 0.86 ($\times 0.864$)	78.92 ± 0.49 ($\times 0.869$)
2	47.78 ± 0.05 ($\times 1.000$)	40.15 ± 0.21 ($\times 0.840$)	40.03 ± 0.05 ($\times 0.843$)
4	25.21 ± 0.06 ($\times 1.000$)	20.45 ± 0.29 ($\times 0.811$)	20.42 ± 0.01 ($\times 0.810$)

Table 4. Training time (in minutes) of SGD, DSGD and DSGD-AC in the WRN28-10 on CIFAR-100 experiments. The communication topology for decentralized methods is the one-peer ring topology. $\times x$ is the relative time compared with synchronous SGD in the same distributed setup.

is widely used in other literature and empirically proven to have a strong correlation (Bisla et al., 2022; Luo et al., 2024).

Across all evaluated setups, DSGD-AC achieves consistently higher test accuracy and lower test loss than both synchronous SGD and decentralized SGD (even under their optimal setups). These results validate the effectiveness and robustness of DSGD-AC across models, topologies, and system scales. The corresponding training curves can be found in Appendix A.4.3. Finally, we validate that DSGD-AC specifically targets flatter minima as DSGD-AC significantly reduces the dominant Hessian eigenvalue compared to standard DSGD. This confirms that the adaptive consensus errors provide implicit sharpness-aware regularization similar to SAM (Foret et al., 2020), but crucially, without the $2\times$ computational overhead required by explicit sharpness minimization methods (Appendix A.4.2 for details).

4.3. Training efficiency

We extend the framework from Wang et al. (2025) for the implementation, and Table 4 shows the training time of our experiments with WRN28-10 and CIFAR-100 using 1, 2 and 4 8×T4 nodes inter-connected by 100Gbps InfiniBand.

In these experiments, decentralized methods require only 0.81–0.87× the training time of synchronous SGD. Compared with DSGD, DSGD-AC introduces negligible additional runtime overhead.

4.4. Summary

DSGD-AC consistently outperforms both DSGD and synchronous SGD in terms of test accuracy and test loss across all evaluated setups. Thanks to its decentralized communication pattern, DSGD-AC can even outperform SGD in terms of runtime performance. Together, these results position DSGD-AC as a compelling alternative to centralized SGD for distributed training.

5. Conclusion

This work challenges the long-standing perception that decentralized training inevitably sacrifices generalization for communication efficiency. Through DSGD-AC, we demonstrate that maintaining controlled consensus errors improves robustness, offering both practical scalability and superior model performance. The method introduces negligible computational overheads and integrates seamlessly with existing decentralized frameworks. These results suggest a paradigm shift: consensus errors should no longer be minimized at all costs but strategically managed as a form of implicit regularization. Beyond immediate applications to deep learning clusters, we envision that the principle of adaptive consensus could inform the design of future large-scale, communication-efficient, and generalizable learning systems. For a more extensive discussion about future potential improvements, please see Appendix A.6.

6. Acknowledgement

The computation and storage resources were enabled by resources provided by the National Academic Infrastructure for Supercomputing in Sweden (NAIIS), partially funded by the Swedish Research Council through grant agreement no. 2022-06725. This work was partially supported by the Wallenberg AI, Autonomous Systems and Software Program (WASP) funded by the Knut and Alice Wallenberg Foundation.

References

- Abadi, M., Barham, P., Chen, J., Chen, Z., Davis, A., Dean, J., Devin, M., Ghemawat, S., Irving, G., Isard, M., et al. TensorFlow: A system for large-scale machine learning. In *12th USENIX symposium on operating systems design and implementation (OSDI 16)*, pp. 265–283, 2016.
- Adam, K. D. B. J. et al. A method for stochastic optimization. *arXiv preprint arXiv:1412.6980*, 1412(6), 2014.
- Alghunaim, S. A. and Yuan, K. A unified and refined convergence analysis for non-convex decentralized learning.

IEEE Transactions on Signal Processing, 70:3264–3279, 2022.

Assran, M., Loizou, N., Ballas, N., and Rabbat, M. Stochastic gradient push for distributed deep learning. In International Conference on Machine Learning, pp. 344–353. PMLR, 2019.

Bellet, A., Tommasi, M., Scaman, K., Neglia, G., et al. Improved stability and generalization guarantees of the decentralized SGD algorithm. In Forty-first International Conference on Machine Learning, 2023.

Benedetti, M. and Ventura, E. Training neural networks with structured noise improves classification and generalization. Journal of Physics A: Mathematical and Theoretical, 57(41):415001, 2024.

Bisla, D., Wang, J., and Choromanska, A. Low-pass filtering SGD for recovering flat optima in the deep learning optimization landscape. In International Conference on Artificial Intelligence and Statistics, pp. 8299–8339. PMLR, 2022.

Bojar, O., Buck, C., Federmann, C., Haddow, B., Koehn, P., Leveling, J., Monz, C., Pecina, P., Post, M., Saint-Amand, H., et al. Findings of the 2014 workshop on statistical machine translation. In Proceedings of the ninth workshop on statistical machine translation, pp. 12–58, 2014.

Defazio, A., Yang, X., Khaled, A., Mishchenko, K., Mehta, H., and Cutkosky, A. The road less scheduled. Advances in Neural Information Processing Systems, 37:9974–10007, 2024.

Dhasade, A., Kermarrec, A.-M., Pires, R., Sharma, R., and Vujasinovic, M. Decentralized learning made easy with decentralizepy. In Proceedings of the 3rd Workshop on Machine Learning and Systems, pp. 34–41, 2023.

Foret, P., Kleiner, A., Mabahi, H., and Neyshabur, B. Sharpness-aware minimization for efficiently improving generalization. arXiv preprint arXiv:2010.01412, 2020.

Gholami, P. and Seferoglu, H. Digest: Fast and communication efficient decentralized learning with local updates. IEEE Transactions on Machine Learning in Communications and Networking, 2:1456–1474, 2024.

Gotmare, A., Keskar, N. S., Xiong, C., and Socher, R. A closer look at deep learning heuristics: Learning rate restarts, warmup and distillation. arXiv preprint arXiv:1810.13243, 2018.

Gur-Ari, G., Roberts, D. A., and Dyer, E. Gradient descent happens in a tiny subspace. arXiv preprint arXiv:1812.04754, 2018.

Huang, K. and Pu, S. Cedas: A compressed decentralized stochastic gradient method with improved convergence. IEEE Transactions on Automatic Control, 2024.

Imfeld, M., Graldi, J., Giordano, M., Hofmann, T., Anagnosidis, S., and Singh, S. P. Transformer fusion with optimal transport. arXiv preprint arXiv:2310.05719, 2023.

Jiang, Y., Neyshabur, B., Mobahi, H., Krishnan, D., and Bengio, S. Fantastic generalization measures and where to find them. arXiv preprint arXiv:1912.02178, 2019.

Kalra, D. S. and Barkeshli, M. Why warmup the learning rate? underlying mechanisms and improvements. Advances in Neural Information Processing Systems, 37: 111760–111801, 2024.

Keskar, N. S., Mudigere, D., Nocedal, J., Smelyanskiy, M., and Tang, P. T. P. On large-batch training for deep learning: Generalization gap and sharp minima. arXiv preprint arXiv:1609.04836, 2016.

Koloskova, A., Stich, S., and Jaggi, M. Decentralized stochastic optimization and gossip algorithms with compressed communication. In International conference on machine learning, pp. 3478–3487. PMLR, 2019.

Kong, L., Lin, T., Koloskova, A., Jaggi, M., and Stich, S. Consensus control for decentralized deep learning. In International Conference on Machine Learning, pp. 5686–5696. PMLR, 2021.

Krizhevsky, A., Hinton, G., et al. Learning multiple layers of features from tiny images. 2009.

Kwon, J., Kim, J., Park, H., and Choi, I. K. ASAM: Adaptive sharpness-aware minimization for scale-invariant learning of deep neural networks. In International conference on machine learning, pp. 5905–5914. PMLR, 2021.

Lanczos, C. An iteration method for the solution of the eigenvalue problem of linear differential and integral operators. Journal of research of the National Bureau of Standards, 45(4):255–282, 1950.

Li, S., Zhao, Y., Varma, R., Salpekar, O., Noordhuis, P., Li, T., Paszke, A., Smith, J., Vaughan, B., Damania, P., et al. Pytorch distributed: Experiences on accelerating data parallel training. arXiv preprint arXiv:2006.15704, 2020.

Li, T., Tao, Q., Yan, W., Lei, Z., Wu, Y., Fang, K., He, M., and Huang, X. Revisiting random weight perturbation for efficiently improving generalization. arXiv preprint arXiv:2404.00357, 2024a.

Li, T., Zhou, P., He, Z., Cheng, X., and Huang, X. Friendly sharpness-aware minimization. In *Proceedings of the IEEE/CVF conference on computer vision and pattern recognition*, pp. 5631–5640, 2024b.

Lian, X., Zhang, C., Zhang, H., Hsieh, C.-J., Zhang, W., and Liu, J. Can decentralized algorithms outperform centralized algorithms? a case study for decentralized parallel stochastic gradient descent. *Advances in neural information processing systems*, 30, 2017.

Lin, T., Karimireddy, S. P., Stich, S. U., and Jaggi, M. Quasi-global momentum: Accelerating decentralized deep learning on heterogeneous data. *arXiv preprint arXiv:2102.04761*, 2021.

Liu, Y., Mai, S., Cheng, M., Chen, X., Hsieh, C.-J., and You, Y. Random sharpness-aware minimization. *Advances in neural information processing systems*, 35:24543–24556, 2022.

Loshchilov, I. and Hutter, F. SGDR: Stochastic gradient descent with warm restarts. *arXiv preprint arXiv:1608.03983*, 2016.

Luo, H., Truong, T., Pham, T., Harandi, M., Phung, D., and Le, T. Explicit eigenvalue regularization improves sharpness-aware minimization. *Advances in Neural Information Processing Systems*, 37:4424–4453, 2024.

Mori, T., Ziyin, L., Liu, K., and Ueda, M. Power-law escape rate of SGD. In *Proceedings of the 39th International Conference on Machine Learning*, volume 162 of *Proceedings of Machine Learning Research*, pp. 15959–15975, 2022. URL <https://proceedings.mlr.press/v162/mori22a.html>.

Papineni, K., Roukos, S., Ward, T., and Zhu, W.-J. Bleu: a method for automatic evaluation of machine translation. In *Proceedings of the 40th annual meeting of the Association for Computational Linguistics*, pp. 311–318, 2002.

Pu, S. and Nedić, A. Distributed stochastic gradient tracking methods. *Mathematical Programming*, 187(1):409–457, 2021.

Singh, S. P. and Jaggi, M. Model fusion via optimal transport. *Advances in Neural Information Processing Systems*, 33:22045–22055, 2020.

Song, M., Ahn, K., and Yun, C. Does SGD really happen in tiny subspaces? *arXiv preprint arXiv:2405.16002*, 2024.

Takezawa, Y., Bao, H., Niwa, K., Sato, R., and Yamada, M. Momentum tracking: Momentum acceleration for decentralized deep learning on heterogeneous data. *arXiv preprint arXiv:2209.15505*, 2022.

Takezawa, Y., Sato, R., Bao, H., Niwa, K., and Yamada, M. Beyond exponential graph: Communication-efficient topologies for decentralized learning via finite-time convergence. *Advances in Neural Information Processing Systems*, 36:76692–76717, 2023.

Vaswani, A., Shazeer, N., Parmar, N., Uszkoreit, J., Jones, L., Gomez, A. N., Kaiser, Ł., and Polosukhin, I. Attention is all you need. *Advances in neural information processing systems*, 30, 2017.

Vogels, T., Karimireddy, S. P., and Jaggi, M. Practical low-rank communication compression in decentralized deep learning. *Advances in Neural Information Processing Systems*, 33:14171–14181, 2020.

Wang, J., Tantia, V., Ballas, N., and Rabbat, M. SlowMo: Improving communication-efficient distributed SGD with slow momentum. *arXiv preprint arXiv:1910.00643*, 2019.

Wang, Z., Jiaojiao, Z., Xuyang, W., and Johansson, M. From promise to practice: realizing high-performance decentralized training. In *The Thirteenth International Conference on Learning Representations*. ICLR, 2025.

Wu, L., Wang, M., and Su, W. J. The alignment property of SGD noise and how it helps select flat minima: A stability analysis. In *Advances in Neural Information Processing Systems*, volume 35, pp. 16843–16857, 2022. URL <https://arxiv.org/abs/2207.02628>.

Ying, B., Yuan, K., Chen, Y., Hu, H., Pan, P., and Yin, W. Exponential graph is provably efficient for decentralized deep training. *Advances in Neural Information Processing Systems*, 34:13975–13987, 2021.

Yuan, K., Chen, Y., Huang, X., Zhang, Y., Pan, P., Xu, Y., and Yin, W. DecentLaM: Decentralized momentum SGD for large-batch deep training. In *Proceedings of the IEEE/CVF International Conference on Computer Vision*, pp. 3029–3039, 2021.

Zagoruyko, S. and Komodakis, N. Wide residual networks. *arXiv preprint arXiv:1605.07146*, 2016.

Zhang, H. R., Li, D., and Ju, H. Noise stability optimization for finding flat minima: A Hessian-based regularization approach. *arXiv preprint arXiv:2306.08553*, 2023.

Zhang, Y., Chen, C., Li, Z., Ding, T., Wu, C., Kingma, D. P., Ye, Y., Luo, Z.-Q., and Sun, R. Adam-mini: Use fewer learning rates to gain more. *arXiv preprint arXiv:2406.16793*, 2024.

Zhou, P., Feng, J., Ma, C., Xiong, C., Hoi, S., and Weinan, E. Towards theoretically understanding why sgd generalizes better than adam in deep learning. arxiv 2020. *arXiv preprint arXiv:2010.05627*, 2010.

Zhu, T., He, F., Zhang, L., Niu, Z., Song, M., and Tao, D. Topology-aware generalization of decentralized SGD. In International Conference on Machine Learning, pp. 27479–27503. PMLR, 2022.

Zhu, T., He, F., Chen, K., Song, M., and Tao, D. Decentralized SGD and average-direction SAM are asymptotically equivalent. In International Conference on Machine Learning, pp. 43005–43036. PMLR, 2023.

Ziyin, L., Liu, K., Mori, T., and Ueda, M. Strength of minibatch noise in SGD. In International Conference on Learning Representations, 2022. URL <https://arxiv.org/abs/2102.05375>.

A. Appendix

A.1. Proof of Proposition 3.1

Recall that

$$\begin{aligned} P &= I - \frac{1}{n} \mathbf{1} \mathbf{1}^\top \\ L &= I - \tilde{W} = U_L \Lambda_L U_L^\top \\ \tilde{G}^{(t)} &= G^{(t)} P U_L \\ Z^{(t)} &= Z^{(t-1)} (I - \gamma^{(t)} \Lambda_L) - \alpha^{(t)} \tilde{G}^{(t)} \end{aligned} \tag{10}$$

where $Z^{(t)}$ describes the consensus error projected onto the eigenbasis of the Laplacian.

Each column $z_k^{(t)}$ of $Z^{(t)}$ evolves as

$$z_k^{(t)} = (1 - \gamma^{(t)} \lambda_k(L)) z_k^{(t-1)} - \alpha^{(t)} \tilde{g}_k^{(t)} \tag{11}$$

where $\lambda_k(L)$ is the k -th eigenvalue of L .

To quantify the dynamics of $\|z_k^{(t)}\|_2^2$, consider a quasi-stationary regime where

$$\mathbb{E}[\tilde{g}_i^{(t)}] = \mu_i, \quad \mathbb{E}[\|\tilde{g}_i^{(t)} - \mu_i\|_2^2] = \sigma_i^2 \tag{12}$$

Then, by taking the expectation on Eq. (11) and letting $m_i = \mathbb{E}[z_i]$, we have

$$m_i = (1 - \gamma^{(t)} \lambda_i(L)) m_i - \alpha^{(t)} \mu_i \tag{13}$$

from which we find (for all modes $i \geq 2$)

$$m_i = -\frac{1}{\lambda_i(L)} \frac{\alpha^{(t)}}{\gamma^{(t)}} \mu_i \tag{14}$$

Next, we define $\tilde{z}_i^{(t)} = z_i^{(t)} - m_i$ so that

$$\tilde{z}_i^{(t)} = (1 - \gamma^{(t)} \lambda_i(L)) \tilde{z}_i^{(t-1)} - \alpha^{(t)} (\tilde{g}_i^{(t-1)} - \mu_i)$$

where we have subtracted m_i from both sides and used the expression for m_i just derived.

Letting $V_i = \mathbb{E}[\|\tilde{z}_i^{(t)}\|_2^2]$ and assuming that the innovation $\eta^{(t-1)} = \tilde{g}_i^{(t-1)} - \mu_i$ is conditionally independent given all events up to iteration $t-1$, we obtain

$$V_i = (1 - \gamma^{(t)} \lambda_i(L))^2 V_i + (\alpha^{(t)})^2 \sigma_i^2.$$

Solving for V_i gives

$$V_i = \frac{(\alpha^{(t)})^2}{1 - (1 - \gamma^{(t)} \lambda_i(L))^2} \sigma_i^2 = \frac{(\alpha^{(t)})^2}{2\lambda_i(L)\gamma^{(t)} - \lambda_i(L)^2(\gamma^{(t)})^2} \sigma_i^2.$$

For t large enough we have $\lambda_i(L)\gamma^{(t)} \leq 1$, so

$$\lambda_i(L)\gamma^{(t)} \leq 2\lambda_i(L)\gamma^{(t)} - \lambda_i(L)^2(\gamma^{(t)})^2 \leq 2\lambda_i(L)\gamma^{(t)}.$$

Consequently,

$$\frac{(\alpha^{(t)})^2}{2\lambda_i(L)\gamma^{(t)}} \sigma_i^2 \leq V_i \leq \frac{(\alpha^{(t)})^2}{\lambda_i(L)\gamma^{(t)}} \sigma_i^2, \tag{15}$$

so in the quasi-stationary regime we have $V_i = \Theta((\alpha^{(t)})^2/\gamma^{(t)})$. Combining (15) with (14) yields

$$\mathbb{E} \left[\|z_i^{(t)}\|_2^2 \right] = V_i + \|m_i\|_2^2 = V_i + \frac{(\alpha^{(t)})^2}{\lambda_i^2(\gamma^{(t)})^2} \|\mu_i\|_2^2.$$

If $\gamma^{(t)} \geq \gamma_{\min} > 0$ and $\alpha^{(t)} \rightarrow 0$, then by (15) we have $V_i \leq (\alpha^{(t)})^2 \sigma_i^2 / (\lambda_i(L)\gamma_{\min}) \rightarrow 0$, and similarly $\|m_i\|_2^2 = O((\alpha^{(t)})^2) \rightarrow 0$. Hence $\mathbb{E} \left[\|z_i^{(t)}\|_2^2 \right] \rightarrow 0$ for each i , so a constant consensus weight $\gamma^{(t)}$ cannot maintain a non-vanishing disagreement radius.

With the schedule $\gamma^{(t)} = g_0(\alpha^{(t)})^p$ and $g_0 > 0$, on the other hand, we obtain the lower bound

$$\mathbb{E} \left[\|z_i^{(t)}\|_2^2 \right] \geq \frac{1}{\lambda_i(L)^2 g_0^2} (\alpha^{(t)})^{2-2p} \|\mu_i\|_2^2 + \frac{1}{2\lambda_i(L)g_0} (\alpha^{(t)})^{2-p} \sigma_i^2.$$

If $p \geq 2$, at least one of the exponents $2 - 2p$ or $2 - p$ is non-positive, so the right-hand side does not converge to zero as $\alpha^{(t)} \rightarrow 0$. Thus for $p \geq 2$ the per-mode energy $\mathbb{E} \left[\|z_i^{(t)}\|_2^2 \right]$ is non-vanishing in the quasi-stationary regime. Finally, since $\|Z^{(t)}\|_F^2 = \|\Delta^{(t)}\|_F^2$ by orthogonality of U , a non-vanishing $\|Z^{(t)}\|_F^2$ implies that $r_t^2 = \mathbb{E} \|\Delta^{(t)}\|_F^2$ is non-vanishing as well.

A.2. Proof of Proposition 3.2

We work in a neighbourhood of a locally strongly convex minimizer x^* of F , with Hessian $H = U_H \Lambda_H U_H^\top$ at x^* and eigenpairs $\{(\lambda_k(H), u_k)\}_{k=1}^d$, $\lambda_k(H) > 0$. Let N be the number of agents and collect the local iterates in

$$X^{(t)} := [x_1^{(t)}, \dots, x_N^{(t)}] \in \mathbb{R}^{d \times N}, \quad X^* := [x^*, \dots, x^*] \in \mathbb{R}^{d \times N}.$$

We denote the communication matrix by W (symmetric, doubly stochastic), and its Laplacian by $L = I - W$.

Let $G^{(t)} = [g_1^{(t)}, \dots, g_N^{(t)}]$ denote the stochastic gradients used at time t , and define the gradient noise

$$\Xi^{(t)} := G^{(t)} - \nabla F(X^{(t-1)}), \quad \nabla F(X^{(t-1)}) := [\nabla f_1(x_1^{(t-1)}), \dots, \nabla f_N(x_N^{(t-1)})].$$

The DSGD-AC update can then be written as

$$X^{(t)} = X^{(t-1)} (I - \gamma^{(t)} L) - \alpha^{(t)} (\nabla F(X^{(t-1)}) + \Xi^{(t)}). \quad (16)$$

Let $P := I - \frac{1}{N} \mathbf{1} \mathbf{1}^\top$ be the projection onto the disagreement subspace, and define the consensus error matrix

$$\Delta^{(t)} := X^{(t)} P,$$

whose columns are precisely the disagreements $\delta_i^{(t)} = x_i^{(t)} - \bar{x}^{(t)}$. Using $LP = PL = L$ (since $L\mathbf{1} = 0$) and multiplying (16) on the right by P yields

$$\Delta^{(t)} = \Delta^{(t-1)} (I - \gamma^{(t)} L) - \alpha^{(t)} \nabla F(X^{(t-1)}) P - \alpha^{(t)} \Xi^{(t)} P. \quad (17)$$

By the i.i.d. local data assumption we have $f_i \equiv F$ for all i and therefore $H_i(x^*) = H$ at the shared minimizer. A first-order Taylor expansion around x^* gives, for each i ,

$$\nabla f_i(x_i^{(t-1)}) = \nabla f_i(x^*) + H(x_i^{(t-1)} - x^*) + r_i^{(t-1)},$$

where the remainder $r_i^{(t-1)}$ is $O(\|x_i^{(t-1)} - x^*\|^2)$. At x^* we have $\nabla f_i(x^*) = 0$, and in a sufficiently small neighbourhood of x^* we may neglect the $r_i^{(t-1)}$ terms, which yields the local approximation

$$\nabla F(X^{(t-1)}) \approx H(X^{(t-1)} - X^*). \quad (18)$$

Since $X^* P = 0$, this implies

$$\nabla F(X^{(t-1)}) P \approx H \Delta^{(t-1)}. \quad (19)$$

Substituting (19) into (17) gives the linearized consensus-error dynamics

$$\Delta^{(t)} \approx \Delta^{(t-1)} (I - \gamma^{(t)} L) - \alpha^{(t)} H \Delta^{(t-1)} - \alpha^{(t)} \Xi^{(t)} P. \quad (20)$$

We now project onto the eigenvectors of H . Let $U_H = [u_1, \dots, u_d]$ collect the eigenvectors of H and $\Lambda_H = \text{diag}(\lambda_1(H), \dots, \lambda_d(H))$. For each k , define the projection of the consensus error onto u_k by

$$\Delta_k^{(t)} := u_k^\top \Delta^{(t)} \in \mathbb{R}^{1 \times N},$$

and the projected noise

$$\xi_k^{(t)} := u_k^\top \Xi^{(t)} P \in \mathbb{R}^{1 \times N}.$$

Left-multiplying (20) by u_k^\top and using $Hu_k = \lambda_k(H)u_k$ yields

$$\Delta_k^{(t)} \approx \Delta_k^{(t-1)}(I - \gamma^{(t)}L) - \alpha^{(t)}\lambda_k(H)\Delta_k^{(t-1)} - \alpha^{(t)}\xi_k^{(t)}. \quad (21)$$

Thus, for each k , the projected consensus error $\Delta_k^{(t)}$ evolves as a linear system on \mathbb{R}^N driven by noise $\xi_k^{(t)}$.

To study stability, we temporarily freeze the stepsizes on a short time window around a fixed time t , writing $\alpha = \alpha^{(t)}$ and $\gamma = \gamma^{(t)}$. Then (21) becomes

$$\Delta_k^{(t)} = \Delta_k^{(t-1)}A_k - \alpha\xi_k^{(t)}, \quad A_k := I - \gamma L - \alpha\lambda_k(H)I.$$

Using $L = I - W$, we can rewrite A_k as

$$A_k = I - \gamma(I - W) - \alpha\lambda_k(H)I = (1 - \gamma - \alpha\lambda_k(H))I + \gamma W. \quad (22)$$

Since W is symmetric and doubly stochastic, its eigenvalues $\{\lambda_j(W)\}_{j=1}^N$ lie in $(-1, 1]$, with $\lambda_1(W) = 1$ because the graph is connected. The eigenvalues of A_k are therefore

$$\mu_{k,j} = 1 - \gamma - \alpha\lambda_k(H) + \gamma\lambda_j(W), \quad j = 1, \dots, N.$$

As A_k is symmetric, mean-square stability of the homogeneous system $\Delta_k^{(t)} = \Delta_k^{(t-1)}A_k$ is equivalent to $|\mu_{k,j}| < 1$ for all j . Thus we require

$$-1 < 1 - \gamma - \alpha\lambda_k(H) + \gamma\lambda_j(W) < 1 \quad \forall j.$$

The right inequality is automatically satisfied for $\alpha > 0$ because $\lambda_1(W) = 1$ and $\lambda_j(W) \leq 1$ imply

$$1 - \gamma - \alpha\lambda_k(H) + \gamma\lambda_j(W) \leq 1 - \alpha\lambda_k(H) < 1.$$

The left inequality is most restrictive for the smallest eigenvalue λ_{\min}^W of W , giving

$$1 - \gamma - \alpha\lambda_k(H) + \gamma\lambda_{\min}(W) > -1 \iff \alpha < \frac{2 + (\lambda_{\min}(W) - 1)\gamma}{\lambda_k(H)}.$$

This is exactly the condition (9).

Since the right-hand side of (9) is strictly decreasing in $\lambda_k(H)$, non-increasing stepsizes $\alpha^{(t)}$ will enter the stable regime for small-curvature modes k earlier along the training trajectory, while high-curvature modes remain closer to instability for longer. In the presence of comparable injected noise, these high-curvature modes therefore sustain larger steady-state variance, which completes the proof.

A.3. Loss envelope and curvature tilt

In this section we relate the consensus errors maintained by DSGD-AC to the local geometry of the global objective. Our goal is to understand which perturbations of the deployed model $\bar{x}(t)$ are implicitly favored or suppressed by the algorithm.

Lemma 1 shows that, in a neighbourhood of a locally strongly convex minimizer x^* , the average local loss decomposes into the loss at the deployed model plus a quadratic envelope term depending on the disagreement covariance Σ_t , up to higher-order corrections. Thus, in this regime, DSGD-AC can be viewed as minimizing $F(\bar{x}(t))$ together with a Hessian-weighted disagreement penalty.

Lemma A.1 (Local loss envelope). *Let x^* be a locally strongly convex minimizer of F with Hessian H at x^* . For a fixed time t , let $\bar{x}(t) := \frac{1}{n} \sum_{i=1}^n x_i^{(t)}$ be the deployed model and define the disagreements $e_i^{(t)} := x_i^{(t)} - \bar{x}(t)$. Let*

$$\Sigma_t := \frac{1}{n} \sum_{i=1}^n e_i^{(t)} e_i^{(t) \top}$$

denote their empirical covariance. Assume that $\|x_i^{(t)} - x^*\|$ is small for all i . Then

$$\frac{1}{n} \sum_{i=1}^n f_i(x_i^{(t)}) = F(\bar{x}(t)) + \frac{1}{2} \text{tr}(H\Sigma_t) + O((\text{tr } \Sigma_t)^{3/2}). \quad (23)$$

Proof. Fix t and abbreviate $\bar{x} = \bar{x}^{(t)}$, $e_i = e_i^{(t)}$. A Taylor expansion of f_i around \bar{x} yields

$$f_i(\bar{x} + e_i) = f_i(\bar{x}) + \nabla f_i(\bar{x})^\top e_i + \frac{1}{2} e_i^\top H e_i + R_i,$$

where $R_i = O(\|e_i\|^3)$ and we used that all f_i have Hessian H at x^* . Averaging over i gives

$$\frac{1}{n} \sum_{i=1}^n f_i(x_i^{(t)}) = F(\bar{x}) + \frac{1}{n} \sum_{i=1}^n \nabla f_i(\bar{x})^\top e_i + \frac{1}{2n} \sum_{i=1}^n e_i^\top H e_i + \frac{1}{n} \sum_{i=1}^n R_i.$$

By definition of \bar{x} we have $\sum_{i=1}^n \delta_i = 0$, hence

$$\frac{1}{n} \sum_{i=1}^n \nabla f_i(\bar{x})^\top e_i = \nabla F(\bar{x})^\top \left(\frac{1}{n} \sum_{i=1}^n e_i \right) = 0.$$

Moreover,

$$\frac{1}{2n} \sum_{i=1}^n e_i^\top H e_i = \frac{1}{2} \text{tr} \left(H \frac{1}{n} \sum_{i=1}^n e_i e_i^\top \right) = \frac{1}{2} \text{tr}(H \Sigma_t).$$

For the remainder, there exists a constant $C > 0$ such that $|R_i| \leq C \|\delta_i\|^3$ in the local region. Thus

$$\left| \frac{1}{n} \sum_{i=1}^n R_i \right| \leq \frac{C}{n} \sum_{i=1}^n \|\delta_i\|^3 \leq C \left(\frac{1}{n} \sum_{i=1}^n \|\delta_i\|^2 \right)^{3/2} = C (\text{tr } \Sigma_t)^{3/2},$$

where the second step follows from Hölder's inequality. This gives the claimed $O((\text{tr } \Sigma_t)^{3/2})$ bound and for the remainder and concludes the proof. \square

To understand how this disagreement penalty depends on curvature and on the communication graph, we diagonalize the local dynamics in the joint eigenbasis of the Hessian and the Laplacian. This leads to the following spectral representation.

Proposition A.2 (Curvature tilt). *Under the assumptions and notation of Proposition 3.2 and Lemma A.1, fix a time t in a local quasi-stationary regime and freeze $\alpha = \alpha^{(t)}$ and $\gamma = \gamma^{(t)}$. Let $L = I - W$ be the graph Laplacian and denote its eigenvalues by $0 = \lambda_1(L) < \lambda_2(L) \leq \dots \leq \lambda_N(L)$, and let $\lambda_1(H) \leq \dots \leq \lambda_d(H)$ be the eigenvalues of H . Let Σ_t be the disagreement covariance at time t . Then the leading-order Hessian-weighted disagreement envelope can be written as*

$$\frac{1}{2} \mathbb{E}[\text{tr}(H \Sigma_t)] \approx \frac{(\alpha^{(t)})^2}{4N} \sum_{j=2}^N \sum_{k=1}^d w_j(\lambda_k(H)) q_{k,j}, \quad (25)$$

where $q_{k,j} \geq 0$ is the innovation variance of the Laplacian–Hessian mode (j, k) and, for $\lambda \geq 0$,

$$w_j(\lambda) := \frac{\lambda}{\gamma^{(t)} \lambda_j(L) + \alpha^{(t)} \lambda}. \quad (26)$$

For each fixed graph mode $j \geq 2$, the weight $w_j(\lambda)$ is strictly increasing in λ .

Proof. We work in the local quadratic regime around x^* and on a short time window around t where we freeze $\alpha = \alpha^{(t)}$ and $\gamma = \gamma^{(t)}$. From the linearization in Appendix A.2 (cf. the proof of Proposition 3.2) we have

$$\Delta^{(s+1)} \approx \Delta^{(s)}(I - \gamma L) - \alpha H \Delta^{(s)} - \alpha \Xi^{(s+1)} P, \quad (24)$$

for s in a short window around t , where $\Xi^{(s+1)}$ collects the gradient noise and P is the projection onto the disagreement subspace.

Let $L = U_L \Lambda_L U_L^\top$ and $H = U_H \Lambda_H U_H^\top$ be the eigendecompositions of the Laplacian and Hessian, with eigenvalues $0 = \lambda_1(L) < \lambda_2(L) \leq \dots \leq \lambda_n(L)$ and $0 < \lambda_1(H) \leq \dots \leq \lambda_d(H)$. We write the consensus error in the joint eigenbasis as

$$\Delta^{(s)} = U_H Y^{(s)} U_L^\top,$$

for some coefficient matrices $Y^{(s)} \in \mathbb{R}^{d \times N}$, and define the corresponding noise coefficients

$$Z^{(s+1)} := U_H^\top \Xi^{(s+1)} P U_L.$$

Substituting these into (24) and using $I - \gamma L = U_L(I - \gamma \Lambda_L)U_L^\top$ and $H = U_H \Lambda_H U_H^\top$ gives

$$Y^{(s+1)} = Y^{(s)}(I - \gamma \Lambda_L) - \alpha \Lambda_H Y^{(s)} - \alpha Z^{(s+1)}.$$

Taking the (k, j) entry yields, for $k = 1, \dots, d$ and $j = 1, \dots, N$,

$$Y_{k,j}^{(s+1)} = a_{k,j} Y_{k,j}^{(s)} - \alpha \zeta_{k,j}^{(s+1)}, \quad a_{k,j} := 1 - \gamma \lambda_j(L) - \alpha \lambda_k(H), \quad (25)$$

where $\zeta_{k,j}^{(s+1)} := Z_{k,j}^{(s+1)}$. Since $\Delta^{(s)}$ lies in the disagreement subspace, the consensus graph mode $j = 1$ does not contribute and we may restrict to $j \geq 2$.

On the short time window around t , we approximate (25) as a stationary AR(1) recursion driven by zero-mean innovations with variance

$$q_{k,j} := \text{Var}(\zeta_{k,j}^{(s)}).$$

Assuming $|a_{k,j}| < 1$ (the stability condition of Proposition 3.2) and that the innovations are uncorrelated across the short time window, the stationary variance $S_{k,j} := \text{Var}(Y_{k,j})$ satisfies the scalar Lyapunov equation

$$S_{k,j} = a_{k,j}^2 S_{k,j} + \alpha^2 q_{k,j},$$

hence

$$S_{k,j} = \frac{\alpha^2}{1 - a_{k,j}^2} q_{k,j}. \quad (26)$$

Using $a_{k,j} = 1 - \gamma \lambda_j(L) - \alpha \lambda_k(H)$, we compute

$$1 - a_{k,j}^2 = 1 - (1 - \gamma \lambda_j(L) - \alpha \lambda_k(H))^2 = 2(\gamma \lambda_j(L) + \alpha \lambda_k(H)) - (\gamma \lambda_j(L) + \alpha \lambda_k(H))^2.$$

In the small-stepsize regime where $\gamma \lambda_j(L) + \alpha \lambda_k(H)$ is small, the quadratic term can be neglected and we obtain the approximation

$$S_{k,j} \approx \frac{\alpha^2}{2(\gamma \lambda_j(L) + \alpha \lambda_k(H))} q_{k,j}. \quad (27)$$

Next, recall that

$$\Sigma_t = \frac{1}{n} \mathbb{E}[\Delta^{(t)} \Delta^{(t)\top}].$$

Using $\Delta^{(t)} = U_H Y^{(t)} U_L^\top$ and orthogonality of U_H and U_L , we obtain

$$\mathbb{E}[\text{tr}(H \Sigma_t)] = \frac{1}{n} \mathbb{E}[\text{tr}(H \Delta^{(t)} \Delta^{(t)\top})] = \frac{1}{n} \mathbb{E}[\text{tr}(\Lambda_H Y^{(t)} Y^{(t)\top})].$$

The last trace equals $\sum_{k=1}^d \lambda_k(H) \sum_{j=1}^n \mathbb{E}[(Y_{k,j}^{(t)})^2]$. Approximating $\mathbb{E}[(Y_{k,j}^{(t)})^2]$ by the stationary variance $S_{k,j}$ in (27) for $j \geq 2$ and noting again that the $j = 1$ consensus mode does not contribute, we obtain

$$\mathbb{E}[\text{tr}(H \Sigma_t)] \approx \frac{\alpha^2}{2n} \sum_{j=2}^n \sum_{k=1}^d \frac{\lambda_k(H)}{\gamma \lambda_j(L) + \alpha \lambda_k(H)} q_{k,j}.$$

Multiplying by $\frac{1}{2}$ yields

$$\frac{1}{2} \mathbb{E}[\text{tr}(H \Sigma_t)] \approx \frac{\alpha^2}{4n} \sum_{j=2}^n \sum_{k=1}^d w_j(\lambda_k(H)) q_{k,j},$$

with

$$w_j(\lambda) := \frac{\lambda}{\gamma \lambda_j(L) + \alpha \lambda},$$

which is exactly (25)–(26).

Finally, for each fixed $j \geq 2$ we have $\lambda_j(L) > 0$ and $\alpha, \gamma > 0$, so for $\lambda \geq 0$,

$$w'_j(\lambda) = \frac{\gamma \lambda_j(L)}{(\gamma \lambda_j(L) + \alpha \lambda)^2} > 0.$$

Thus $w_j(\lambda)$ is strictly increasing in λ for every $j \geq 2$, which completes the proof. \square

The spectral form in Proposition 3 separates the envelope into curvature-dependent weights $w_j(\lambda_k(H))$ and mode-wise innovation variances $q_{k,j}$. To go further, we specialize to the case where these innovations arise from mini-batch SGD noise. A growing body of empirical and theoretical work has shown that, near a local minimum, the covariance of mini-batch SGD gradients is approximately Hessian-aligned and scales with both the loss value and curvature, $\text{Cov}(g(x) - \nabla F(x)) \approx c_t L(x) H(x)$, in linear models and deep networks (e.g., [Ziyin et al. \(2022\)](#); [Wu et al. \(2022\)](#); [Mori et al. \(2022\)](#)). Under this structure, the $q_{k,j}$ inherit the same dependence on the Hessian eigenvalues, which yields a curvature-dependent spectral penalty of the form in (29).

Corollary A.3 (Hessian-aligned mini-batch noise). *Under the assumptions and notation of Proposition A.2, assume in addition that the gradient noise driving DSGD-AC is inherited from a mini-batch SGD oracle whose covariance is approximately Hessian-aligned,*

$$\text{Cov}(g_i(x) - \nabla f_i(x)) \approx c_t L(x) H(x), \quad (28)$$

for some scalar factor $c_t > 0$ depending on the batch size and possibly on time t . Then, in the local quadratic regime around x^* , the leading-order Hessian-weighted disagreement envelope can be written as

$$\frac{1}{2} \mathbb{E}[\text{tr}(H \Sigma_t)] \approx L(\bar{x}^{(t)}) \sum_{k=1}^d \omega_t(\lambda_k(H)), \quad (29)$$

where $\omega_t : [0, \infty) \rightarrow [0, \infty)$ is strictly increasing and satisfies that $\lambda \mapsto \omega_t(\lambda)/\lambda$ is also strictly increasing on $(0, \infty)$. In particular, larger Hessian eigenvalues receive a disproportionately larger penalty relative to their magnitude than smaller ones.

Proof. By Proposition A.2, the leading-order envelope can be written as

$$\frac{1}{2} \mathbb{E}[\text{tr}(H \Sigma_t)] \approx \frac{(\alpha^{(t)})^2}{4n} \sum_{j=2}^n \sum_{k=1}^d w_j(\lambda_k(H)) q_{k,j},$$

with

$$w_j(\lambda) = \frac{\lambda}{\gamma^{(t)} \lambda_j(L) + \alpha^{(t)} \lambda},$$

and $q_{k,j}$ the innovation variances of the joint Laplacian–Hessian modes. Under the Hessian-aligned covariance structure (28), the per-step gradient noise covariance in the Hessian eigenbasis is approximately diagonal with entries proportional to $L(\bar{x}^{(t)}) \lambda_k(H)$. Projecting into the joint basis, the $q_{k,j}$ inherit this alignment and, up to graph-dependent constants, satisfy

$$q_{k,j} \approx c_t L(\bar{x}^{(t)}) \lambda_k(H).$$

Substituting this scaling gives

$$\frac{1}{2} \mathbb{E}[\text{tr}(H \Sigma_t)] \approx L(\bar{x}^{(t)}) \frac{(\alpha^{(t)})^2 c_t}{4N} \sum_{j=2}^N \sum_{k=1}^d \frac{\lambda_k(H)^2}{\gamma^{(t)} \lambda_j(L) + \alpha^{(t)} \lambda_k(H)}.$$

and we recover (29). with

$$\omega_t(\lambda) := \frac{(\alpha^{(t)})^2 c_t}{4N} \sum_{j=2}^N \frac{\lambda^2}{\gamma^{(t)} \lambda_j(L) + \alpha^{(t)} \lambda}.$$

It remains to verify the monotonicity properties of ω_t . For each fixed $j \geq 2$, define

$$h_{t,j}(\lambda) := \frac{\lambda^2}{\gamma^{(t)} \lambda_j(L) + \alpha^{(t)} \lambda} = \lambda w_j(\lambda),$$

where $w_j(\lambda)$ is the weight from Proposition A.2. We have already shown that, for $\lambda \geq 0$, $w_j(\lambda) \geq 0$ and $w_j(\lambda)$ is strictly increasing. Therefore, for $\lambda > 0$,

$$h'_{t,j}(\lambda) = w_j(\lambda) + \lambda w'_j(\lambda) > 0,$$

so each $h_{t,j}$ is strictly increasing on $(0, \infty)$ (and nondecreasing on $[0, \infty)$). Since ω_t is a positive linear combination of the $h_{t,j}$, $\omega_t(\lambda)$ is strictly increasing on $(0, \infty)$. Moreover,

$$\frac{\phi_t(\lambda)}{\lambda} = \frac{(\alpha^{(t)})^2 c_t}{4n} \sum_{j=2}^n \frac{\lambda}{\gamma^{(t)} \lambda_j(L) + \alpha^{(t)} \lambda} = \frac{(\alpha^{(t)})^2 c_t}{4n} \sum_{j=2}^n w_j(\lambda).$$

Each $w_j(\lambda)$ is strictly increasing in λ by Proposition A.2, so their positive linear combination $\omega_t(\lambda)/\lambda$ is also strictly increasing on $(0, \infty)$. This proves the monotonicity stated in the corollary. \square

Remark The spectral form in (29) shows that, under Hessian-aligned mini-batch noise, the leading-order loss inflation induced by DSGD-AC behaves like an implicit spectral penalty of the form $L(\bar{x}(t)) \sum_k \omega_t(\lambda_k(H))$, where both $\omega_t(\lambda)$ and $\omega_t(\lambda)/\lambda$ are strictly increasing. In particular, larger eigenvalues of H are penalized disproportionately more per unit curvature than smaller ones. This contrasts with classical criteria that depend only on $\text{tr}(H)$ or $\log \det H$, and implies that the top eigenvalues of H are implicitly regularized by the combination of consensus noise and mini-batch SGD. Conceptually, this connects DSGD-AC to explicit eigenvalue regularization schemes that aim to control large curvature directions in sharpness-aware methods such as Eigen-SAM (Luo et al., 2024) or Hessian-based noise-stability regularization (Zhang et al., 2023), but here the regularization arises automatically from decentralized averaging and stochastic gradients rather than from additional optimization steps.

A.4. Additional experiments

A.4.1. ADAPTIVE CONSENSUS WITH DECENTRALIZED ADAM

We also validate the idea of controlling consensus errors on transformer models by simply replacing the local update with the Adam optimizer (Adam et al., 2014). DSGD-AC is then adapted to DAdam-AC as in Algorithm 2.

Algorithm 2: Decentralized Adam with adaptive consensus (DAdam-AC) on worker i

Data: Dataset (D), the number of workers (N), the number of epoch (E), the number of batches per epoch (T), initialization ($x^{(0)}$), and a hyperparameter ($p \in \mathbb{R}^+$).

Result: Deployed model $\bar{x} = \frac{1}{n} \sum_{j=1}^n x_j^{(TE)}$

$x_1^{(0)} = x_2^{(0)} = \dots = x_n^{(0)} = x^{(0)}$

for $t = 1$ to TE **do**

$$\begin{aligned} g_i^{(t)} &= \nabla f(x_i^{(t-1)}; s_i^{(t)}) \\ m_i^{(t)} &= \beta_1 m_i^{(t)} + g_i^{(t)} \\ v_i^{(t)} &= \beta_2 v_i^{(t)} + g_i^{(t)} \odot g_i^{(t)} \\ \hat{m}_i^{(t)} &= m_i^{(t)} / (1 - \beta_1^t) \\ \hat{v}_i^{(t)} &= v_i^{(t)} / (1 - \beta_1^t) \\ \gamma^{(t)} &= [\alpha^{(t)} / \alpha_{\max}]^p \\ x_i^{(t)} &= x_i^{(t-1)} - \alpha^{(t)} \frac{\hat{m}_i^{(t)}}{\hat{v}_i^{(t)}} + \gamma^{(t)} \sum_{j \in \mathcal{N}(i)} W_{ij} (x_j^{(t-1)} - x_i^{(t-1)}) \end{aligned}$$

end

We train Transformer (the big variant, $\sim 213M$ parameters) (Vaswani et al., 2017) on WMT14 (English-to-German) (Bojar et al., 2014) and present the curves of training losses and BLEU scores on the test set. The BLEU scores (Papineni et al., 2002) (which is used to evaluate the translation quality in the original paper) and the losses on the test set and the training set are reported in Table 5.

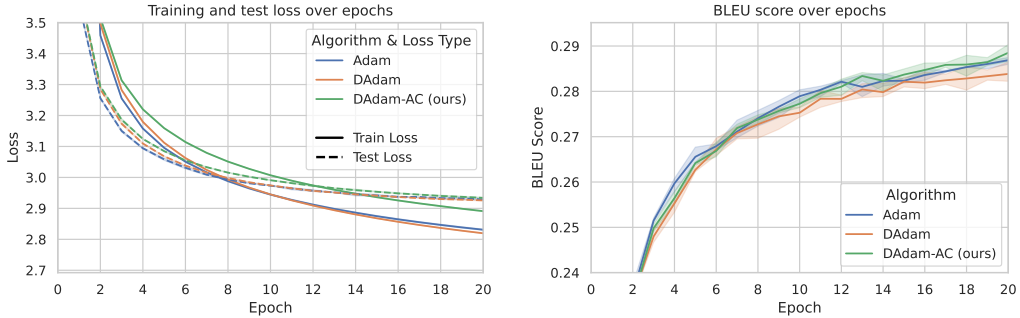


Figure 5. Transformer (big) on WMT14 English-to-German. **Left:** Losses on training set. **Right:** BLEU scores on the test set.

Algorithm	BLEU score \uparrow	Test loss \downarrow	Train loss \downarrow
Adam	28.68 ± 0.07	2.9290 ± 0.0026	2.8310 ± 0.0019
DAdam	28.38 ± 0.22	2.9258 ± 0.0018	2.8195 ± 0.0008
DAdam-AC	28.89 ± 0.17	2.9205 ± 0.0020	2.8456 ± 0.0016

Table 5. Performance comparison of DAdam, Adam, and DAdam-AC on neural machine translation with the transformer model.

The results demonstrate that DAdam-AC can outperform other baselines on the translation quality metric and the test loss. The adaptive consensus enhances the decentralized Adam. We believe further improvement is possible if we take the adaptive consensus into account when designing the optimizer (see the discussion in Appendix A.6).

A.4.2. SHARPNESS-AWARE MINIMIZATION

Even though comparing DSGD-AC with explicit sharpness-aware minimization (SAM) methods is not our emphasis, we implement SAM (Foret et al., 2020) and report its results with 8 workers for reference. We follow Foret et al. (2020) to use $\rho = 0.05$ in all the experiments. In the experiment results, SAM achieves the best test accuracy, test loss, and top-1 eigenvalue of the Hessian. However, it should be noted that SAM introduces $2\times$ computation cost, and, since it is not numerically stable under the mixed precision training (the loss becomes NaN in around 30 epochs), it takes $\sim 4\times$ training time as the synchronous SGD in the 8-worker setup.

Model	Test accuracy \uparrow	Test loss \downarrow	Train loss \downarrow	Top-1 eigenvalue \downarrow
WRN28-10	83.05 ± 0.26	0.697 ± 0.010	0.050 ± 0.001	0.028 ± 0.001
WRN16-8	81.05 ± 0.09	0.752 ± 0.003	0.088 ± 0.001	0.154 ± 0.007

Table 6. Performance SAM on image classification tasks on CIFAR-100.

A.4.3. TRAINING CURVES

This section presents the training curves of the experiments included in Table 1. Figures 6, 7, 8, 9, 10, and 11 (*in the next page*) present the training loss, the test loss, and the test accuracy along the training.

The effect of adaptive consensus can be directly observed at the corresponding E_{start} .

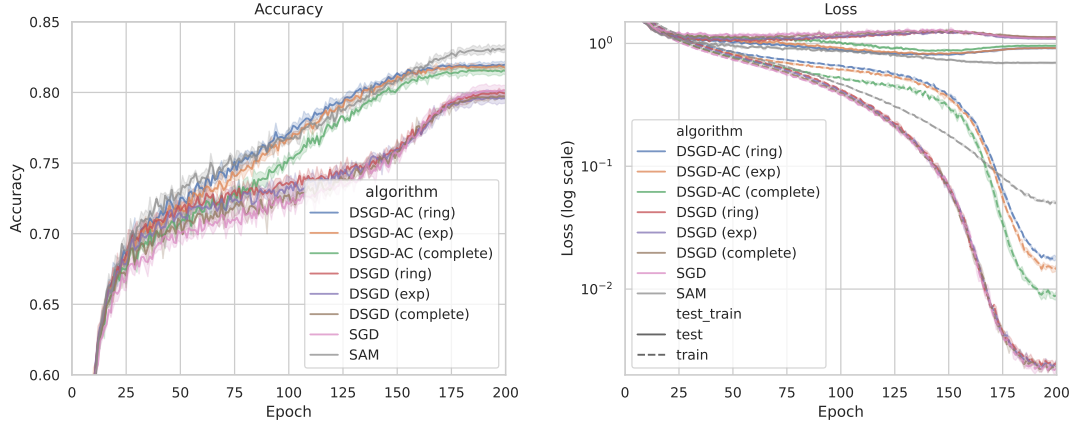


Figure 6. WRN28-10 on CIFAR-100 with 8 workers. **Left:** Test accuracy on test set. For decentralized training, the accuracy is evaluated on the global average model. **Right:** Training and test losses.

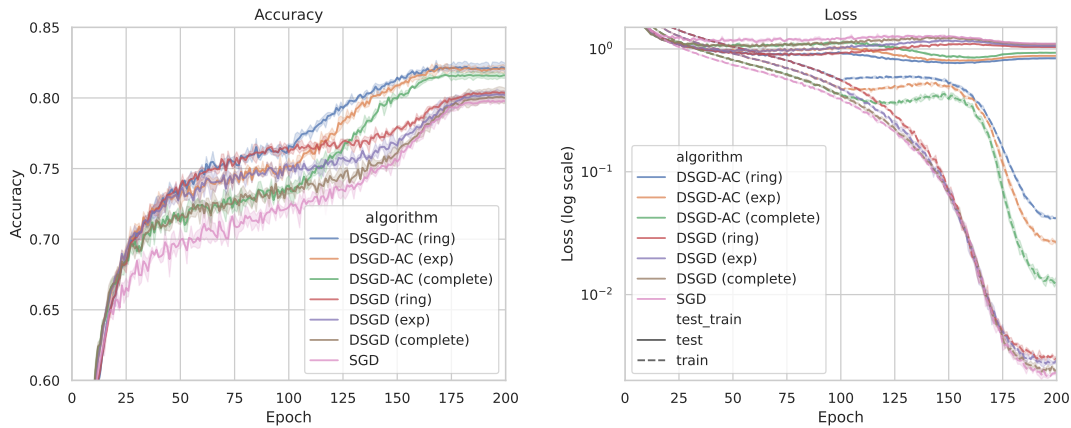


Figure 7. WRN28-10 on CIFAR-100 with 16 workers. **Left:** Test accuracy on test set. For decentralized training, the accuracy is evaluated on the global average model. **Right:** Training and test losses.

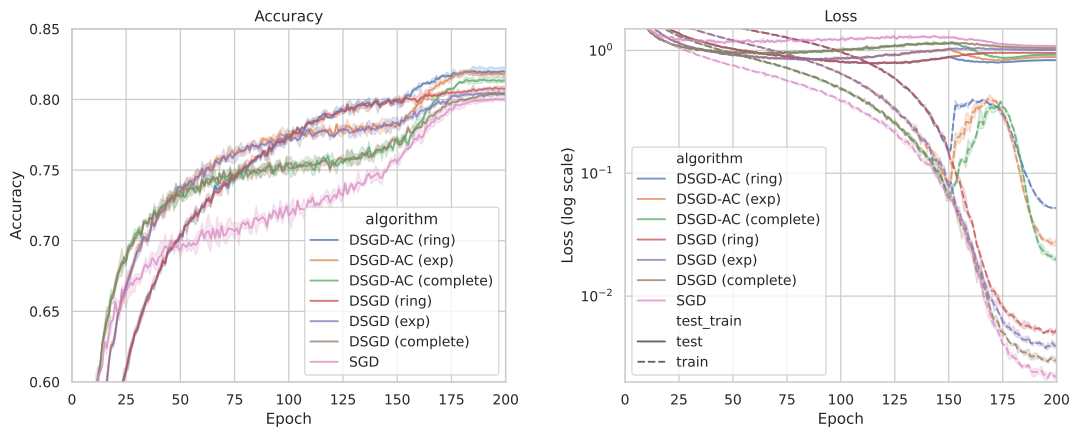


Figure 8. WRN28-10 on CIFAR-100 with 32 workers. **Left:** Test accuracy on test set. For decentralized training, the accuracy is evaluated on the global average model. **Right:** Training and test losses.

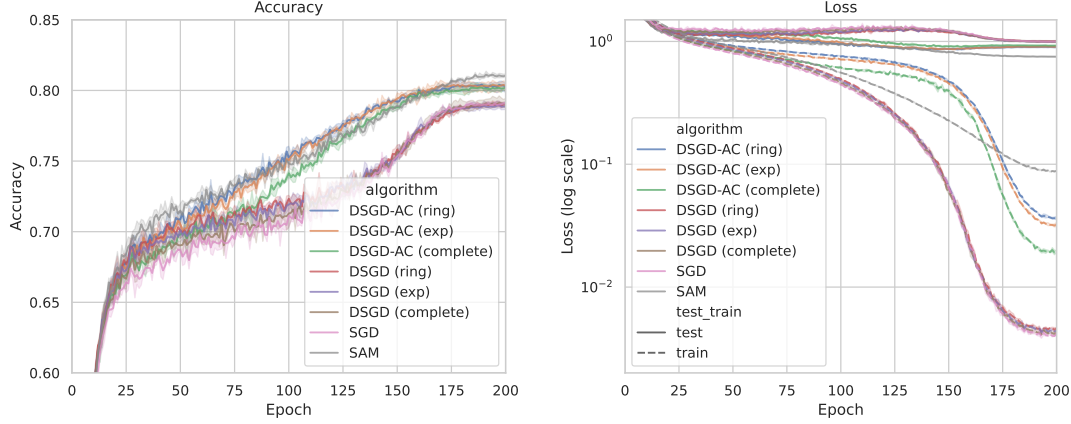


Figure 9. WRN16-8 on CIFAR-100 with 8 workers. **Left:** Test accuracy on test set. For decentralized training, the accuracy is evaluated on the global average model. **Right:** Training and test losses.

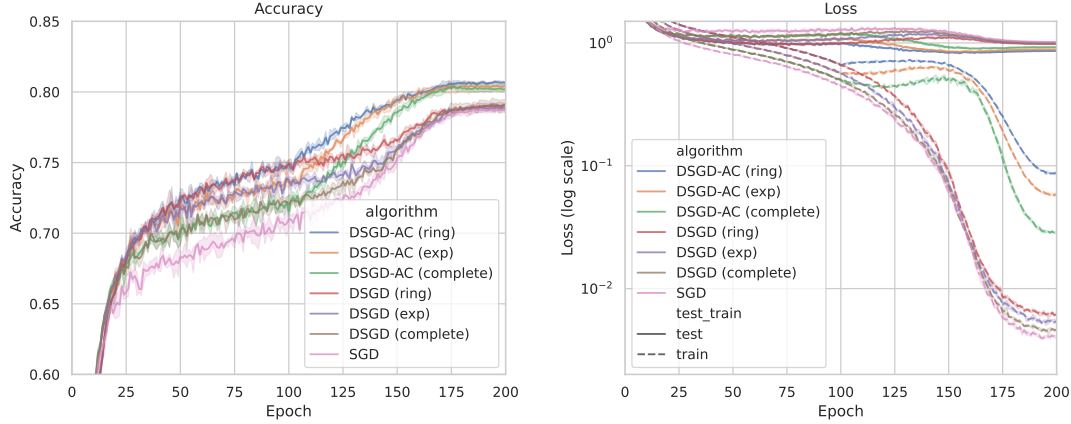


Figure 10. WRN16-8 on CIFAR-100 with 16 workers. **Left:** Test accuracy on test set. For decentralized training, the accuracy is evaluated on the global average model. **Right:** Training and test losses.

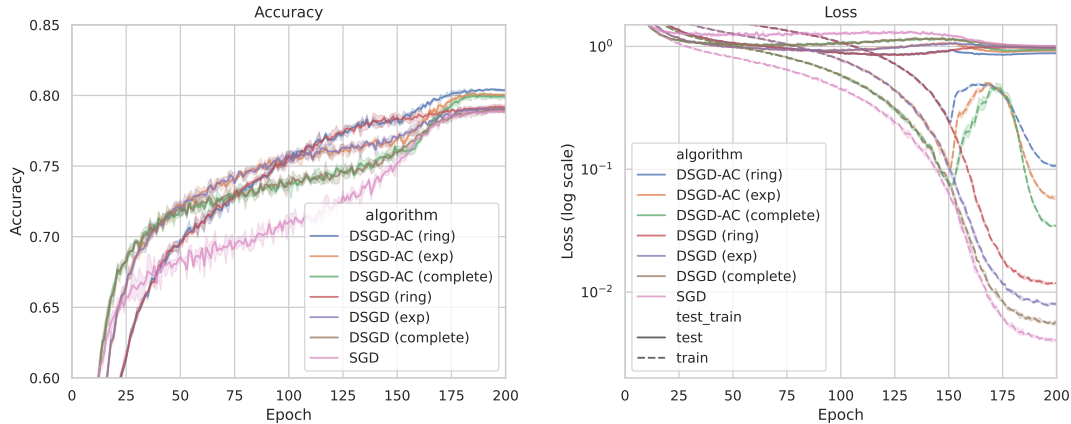


Figure 11. WRN16-8 on CIFAR-100 with 32 workers. **Left:** Test accuracy on test set. For decentralized training, the accuracy is evaluated on the global average model. **Right:** Training and test losses.

A.4.4. SENSITIVITY ANALYSIS OF p

This section presents the complete sensitivity analysis of the parameter p in the setup with 8 workers and the one-peer ring topology. The training curves (test accuracy, test loss, and training loss) with $p = \{0, 1, 2, 3, 4, 5\}$ are presented in Figure 12, and the final metrics are presented in Table 7. The tracked average norm of consensus errors with varying p is shown in Figure 4.

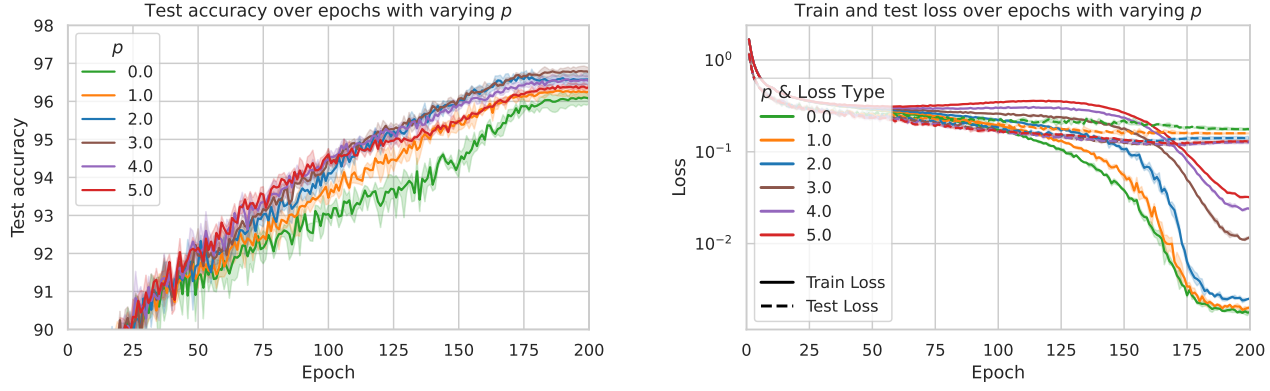


Figure 12. DSGD(-AC) on WRN28-10 on CIFAR-10 with varying p . **Left:** Test accuracy on test set. For decentralized training, the accuracy is evaluated on the global average model. **Right:** Training and test losses.

p	Test Accuracy (%) \uparrow	Train Loss \downarrow	Test Loss \downarrow
0	96.07 ± 0.13	0.002 ± 0.000	0.176 ± 0.005
1	96.26 ± 0.14	0.002 ± 0.000	0.159 ± 0.003
2	<u>96.58 ± 0.18</u>	0.003 ± 0.000	0.141 ± 0.006
3	96.77 ± 0.11	0.012 ± 0.000	<u>0.128 ± 0.003</u>
4	<u>96.53 ± 0.13</u>	0.024 ± 0.001	0.127 ± 0.004
5	96.37 ± 0.04	0.032 ± 0.001	0.130 ± 0.002

Table 7. Sensitivity analysis of parameter p in the WRN28-10 on CIFAR10 experiment. The best value is **bold**, and the second best is underlined.

A.4.5. SENSITIVITY ANALYSIS OF E_{START}

In this section, we vary the epoch in which we enable the adaptive consensus (AC). We test the performance of DSGD-AC with starting epochs {10 (*default*), 50, 100, 170, 200 (*equivalent to DSGD*)}, for different worker counts {16, 32} and topologies {complete, exponential graph, one-peer ring}.

In the experiments, we fix $p = 3$, and α_{max} is taken as the learning rate at the start of the epoch when AC is enabled (α is monotonically decreasing after the warm-up phase, so γ is always kept in $[0, 1]$).

Figures 14-16 show the test accuracies and test losses of DSGD-AC with various E_{start} and their comparison with the synchronous SGD baselines.

Interpretation of the results:

- For the case with larger number of workers (32) and poor connectivity in the communication topology, delaying the activation of AC can bring better performance compared to the default setup.
- As shown in Figures 13-16, DSGD-AC can achieve both better test accuracy and better test loss than decentralized SGD and synchronous SGD on at least one starting epoch (that is not 200) on all setups. This implies that the AC mechanism can improve the generalization.

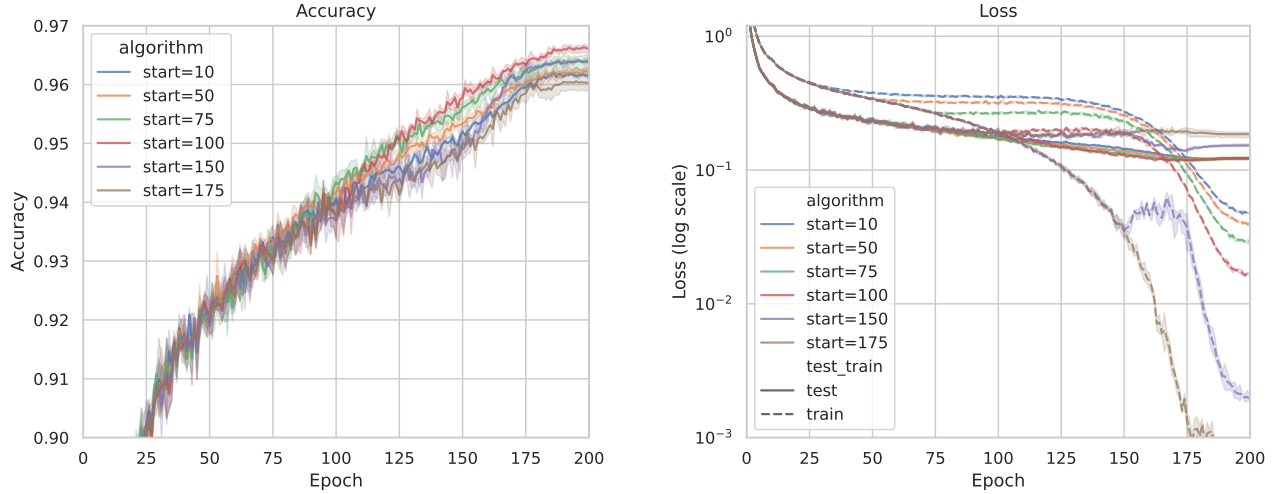


Figure 13. DSGD-AC on WRN28-10 on CIFAR-10 with varying E_{start} with 16 workers and one-peer ring topology. **Left:** Test accuracy on test set. For decentralized training, the accuracy is evaluated on the global average model. **Right:** Training and test losses.

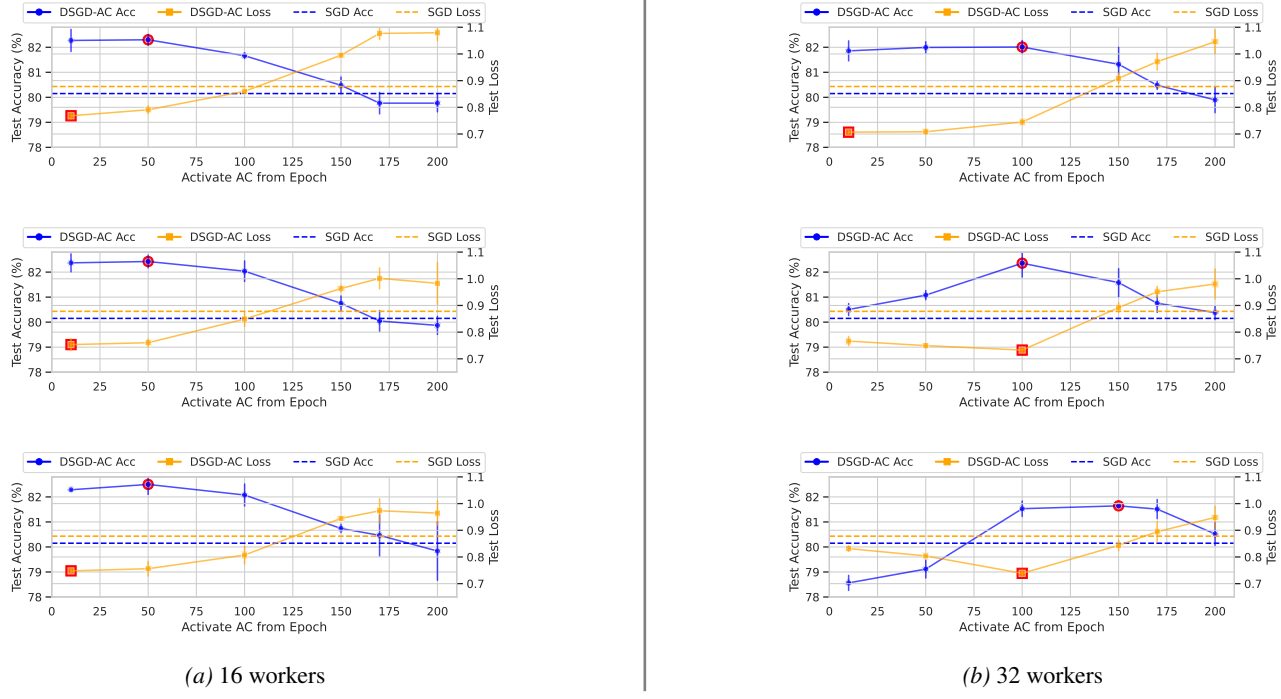


Figure 14. WRN28-10 on CIFAR100. The global batch size 128. Figures from top to bottom correspond to complete, exponential graph, and one-peer ring, respectively. The best test accuracy and the best test loss are highlighted by red marks.

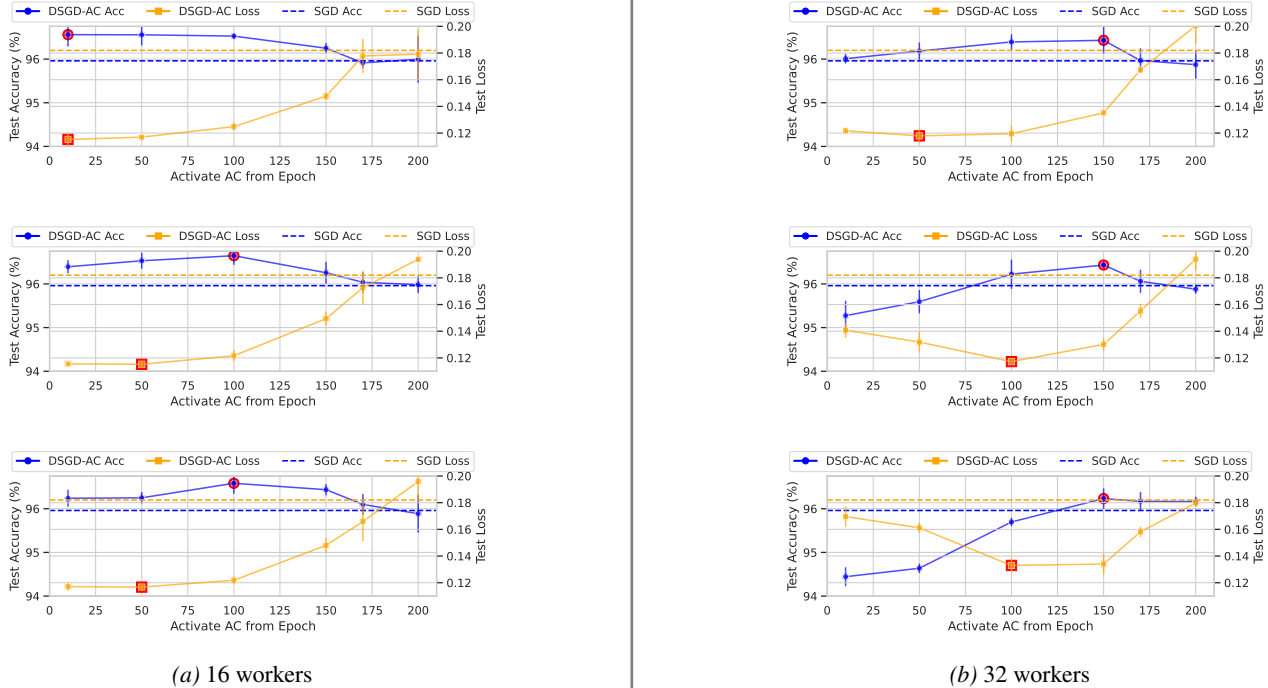


Figure 15. WRN28-10 on CIFAR10. The global batch size 128. Figures from top to bottom correspond to complete, exponential graph, and one-peer ring, respectively. The best test accuracy and the best test loss are highlighted by red marks.

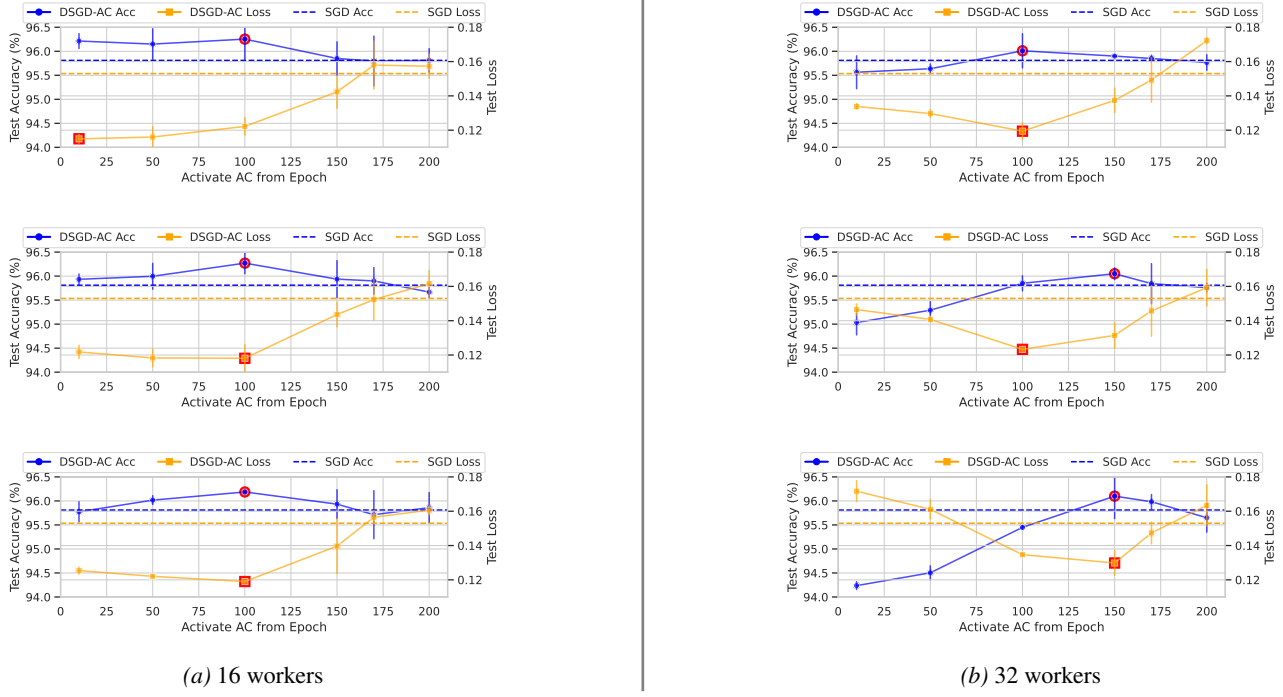


Figure 16. WRN16-8 on CIFAR10. The global batch size 128. Figures from top to bottom correspond to complete, exponential graph, and one-peer ring, respectively. The best test accuracy and the best test loss are highlighted by red marks.

A.5. Training and evaluation details

A.5.1. HYPERPARAMETERS FOR IMAGE CLASSIFICATION EXPERIMENTS WITH WRN ON CIFAR10/100

The selection of hyperparameters follows the original paper (Zagoruyko & Komodakis, 2016), and our baseline implementation perfectly matches its performance.

Category	Setting
General	
Number of epochs	200
Global batch size	128 for 8-worker setup and it is linearly scaled with the number of workers.
Learning rate scheduler	Linearly warm-up to α_{\max} in the first 10 epochs, followed by the cosine annealing until the end. $\alpha_{\max} = 0.1$ for 128 batch size, and it is linearly scaled with the batch size.
Base optimizer	SGD with momentum $\beta = 0.9$ and weight decay 5×10^{-4} .
Data shuffle	Randomly shuffled and split into N local datasets each epoch.
Decentralized training	
Number of workers	8, 16, and 32
Communication topology	One-peer ring (alternating between neighbors $i - 1$ and $i + 1$ across iterations), one-peer exponential (Ying et al., 2021), and complete graph (global all-reduce among all workers).
DSGD-AC parameters	Exponent $p = 3$ (tuned based on experiments); $\gamma = 1$ before E_{start} .
BatchNorm calibration	Similar to the case in (Defazio et al., 2024), a calibration on the BatchNorm statistics is needed because there is a mismatch between the local models and the global average. To calibrate mismatched statistics, a full pass over the training set is conducted before validation. Only one calibration should be done if intermediate checkpoints are not evaluated. Note that we also apply the calibration to synchronous SGD for a fair comparison.

A.5.2. HYPERPARAMETERS FOR NEURAL MACHINE TRANSLATION EXPERIMENTS WITH TRANSFORMER ON WMT14

The selection of hyperparameters follows the original paper (Vaswani et al., 2017), and our baseline implementation perfectly matches its performance.

Category	Setting
General	
Number of epochs	20
Global batch size	$\sim 50k$ tokens including both source and target texts
Learning rate scheduler	Linear warm-up to 5×10^{-4} over the first 4000 iterations, then decay as $\alpha_0 \cdot (4000/t)^{0.5}$ (t is the iteration index). $\alpha_0 = 0.0005$ for centralized Adam, and $\alpha_0 = 0.0013$ for decentralized methods.
Base optimizer	Adam ($\beta_1 = 0.9$, $\beta_2 = 0.98$) for centralized Adam, and ($\beta_1 = 0.974$, $\beta_2 = 0.999$) for decentralized methods.
Data shuffle	Randomly shuffled and split into N local datasets each epoch
Decentralized training	
Number of workers	8
Communication topology	One-peer ring (alternating between neighbors $i - 1$ and $i + 1$ across iterations)
DSGD-AC parameters.	Exponent $p = 2$ (tuned based on experiments); $\gamma = 1$ during warm-up.
Normalization	Since only layer normalization is used, no calibration is needed.

A.5.3. EVALUATION DETAILS

Top-1 eigenvalue evaluation We use Lanczos algorithm (Lanczos, 1950) for efficient evaluation of the top-1 eigenvalue of the Hessian. To be specific, the loss function is

$$F(x) = \frac{1}{|\mathcal{S}|} \sum_{b=1}^B f(x; s_b) \quad (28)$$

where s_b denotes a batch of samples from the training set, \mathcal{S} denotes the total number of samples in the training set, and $\{s_1, \dots, s_B\}$ collectively cover the entire training set. To exclude the impact of mismatched statistics in the batch normalization layers, we evaluate the Hessian-vector product in training mode and carefully control the random seed to ensure that the sample order, batching, and data augmentation are identical across all evaluations.

We fix the number of Lanczos iterations to 15, which is sufficient for an accurate evaluation.

A.6. Discussion

Future improvement directions The practicality in the adaptive consensus mechanism motivates the following future directions:

- Compression for communication–alignment tradeoffs. While communication compression in decentralized training has been widely studied (Koloskova et al., 2019; Vogels et al., 2020; Huang & Pu, 2024), most methods aim to approximate centralized training. DSGD-AC suggests a different view: small $\gamma^{(t)}$ and the alignment in Proposition 3.2 may benefit generalization. This opens the possibility of designing compressors that (i) spend more communication budget early in training when alignment forms, or (ii) implicitly maintain updates along high-curvature directions to further strengthen the alignment of disagreement with the dominant Hessian subspace.
- Decentralized mixing for better alignment. Current decentralized mixing relies on simple weighted averaging. Under DSGD-AC, one may interpret the disagreement as a curvature-related perturbation around the global model. This motivates exploring new mixing rules that selectively damp low-curvature disagreement while keeping high-curvature components active, thereby enhancing the “curvature tilt” observed in the algorithm. Such rules would be complementary to the compressors described above.
- Model fusion. Model fusion (Singh & Jaggi, 2020; Imfeld et al., 2023) combines models trained along different trajectories. For standard DSGD, their impact is limited because consensus errors quickly vanish, and the matching among parameters from local models is trivial. In DSGD-AC, however, the disagreement remains non-negligible, making model fusion a potential alternative to simple averaging, possibly improving performance.

Combine Adaptive consensus with adaptive optimizers In adaptive optimizers like Adam, the update is scaled by the inverse of the moving average of the componentwise square of the gradients. The scaling in each gradient coordinate eliminates the anisotropic structure in gradient noise (Zhou et al., 2010), which conflicts with the purpose of the AC mechanism which instead tends to enhance the structure. Since consensus errors are the accumulated updates after the scaling, the analysis in this paper may not directly work on the case that directly combines AC with adaptive optimizers. It can be an interesting direction for future work to find better ways for AC to co-exist with adaptive optimizers, possibly by recovering/extracting noise structure from the consensus errors. For example, designing the AC with variants like Adam-mini (Zhang et al., 2024) can be a practical idea for efficiently recovering the noise structure in the consensus errors.